Rhenium and Iridium Complexes and Their Interaction with DNA

Humaira Patel

February 2023

Department of Chemistry

E-mail: h.patel15@lancaster.ac.uk

Keywords: DNA, Transition-Metals, Rhenium, Iridium

Abstract

The Fletcher group has previously explored the ruthenium complexes of 4,4'-bis(benzoxazole-2-yl)-2,2'-bipyridine (BBOB), 4,4'-bis(benzothiazole-2-yl)-2,2'-bipyridine (BBTB), and 4,4'-bis(benzimidazole-2-yl-2,2'-bipyridine (BBIB) and shown that they typically bind in the minor groove of DNA, rather than intercalate, having a preference for defect sites such as bulges and hairpin loops.

We report here the synthesis of a series of related ligands, and their complexation to both rhenium(I) and iridium(III), via reaction with $Re(CO)_5Br$ and $\{Ir(ppy)_2(\mu\text{–}Cl)\}_2$ respectively. These have been characterized through NMR, infrared and UV-Vis absorption and emission spectroscopy, illustrating the effect of conjugation of the extended heterocyclic structure. Despite solubility issues, we will discuss here the photophysical analysis, including circular dichroism (CD) spectroscopic studies, which show that these complexes interact with DNA and highlight a new potential DNA binding mode.

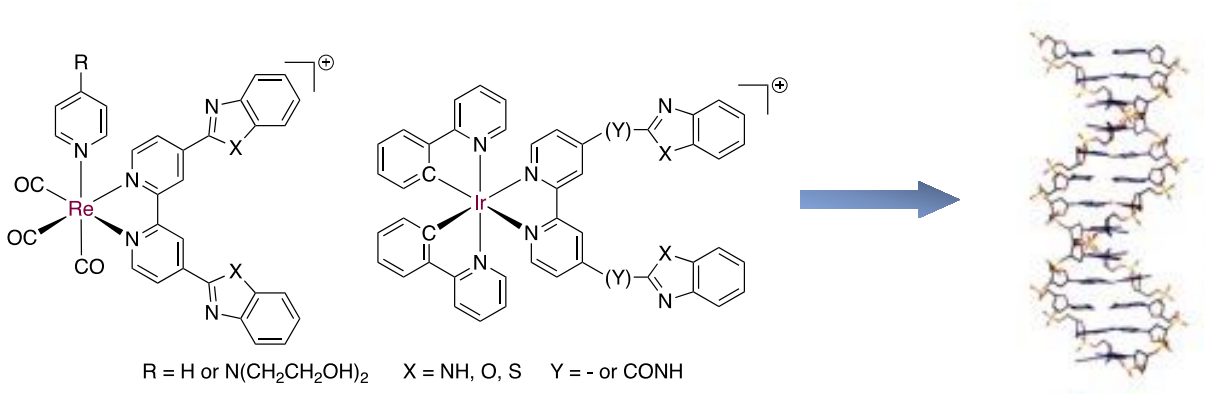

Acknowledgements

Firstly I would like to thanks Dr.Nick Fletcher for being my supervisor and for the time and effort he has placed in order for me to complete this. He has taught me so many skills and always gone out of his way to help, I appreciate it so much! As well as all members of the Fletcher group for their contribution of ideas to help me to progress with my work.

Also would like to thank Dr. Mike Coogan for helping me throughout the project when I needed advice as well as being such a big part by supplying the solubility ligand.

And would like to thank all the other members in the department who have helped and supported me through my masters!

Also to my mum, siblings and the rest of my family and friends who have always been there to support and encourage me.

Contents Page

Glossary

BBOB (4,4’-bis(benzoxazol-2-yl)-2,2’-bipyridine),

BBTB 4,4’-bis(benzothiazol-2-yl)-2,2’-bipyridine)

BBIB 4,4’-bis(benzimidazole-2-yl)-2,2’-bipyridine

CD Circular Dichroism

COSY ^{1}H Correlated Spectroscopy

CT-DNA Calf Thymus DNA

DMF Dimethylformamide

DMSO Dimethylsulfoxide

DNA Deoxyribonucleic Acid

LC Ligand to charge

LMCT Ligand to metal charge transfer

MLCT Metal to ligand charge transfer

NMR Nuclear magnetic resonance

RNA Ribonucleic acid

T *N*,*N*-bis(2-hydroxyethyl)-4-Pyridinecarboxamide

UV-Vis Ultraviolet Visible

1. Introduction

1.1 Overview

DNA (or deoxyribose nucleic acid) is one of the most fascinating and beautiful molecular architectures, which provides the blue print and chemical information, or programme, for all living things, in all of their wonderful diversity.[1] It is, in its simplest form, a biopolymer composed of a series of four nucleotide monomers. Each of these comprise of a combination of three basic building blocks: a planar aromatic derivative, either a pyrimidine or purine base, a deoxyribose sugar, and a phosphate group. There are two purine bases, adenine (A) and guanine (G) which conjugate through hydrogen bonding with two pyrimidine bases thymine (T) and cytosine (C) respectively. (Figure 1) Each nucleotide is then joined with two other nucleotides in a polymeric chain through a phosphodiester bond linking the 5'-end of the sugar to the 3'-end of the adjacent nucleotide sugar. (Figure 2) Hence the polymerisation of nucleotides results in a single-stranded polyanionic chain resulting in the primary structure. The DNA chain contains "the sequence" of these four nucleobases which contains the precise information to carry out the functions of a cell. DNA then adopts a double stranded helical structure by the formation of hydrogen bonds between bases on the opposing anti-parallel strands; Watson-Crick base-pairing. This allows A and T to pair through two hydrogen bonds and G and C through three hydrogen bonds.

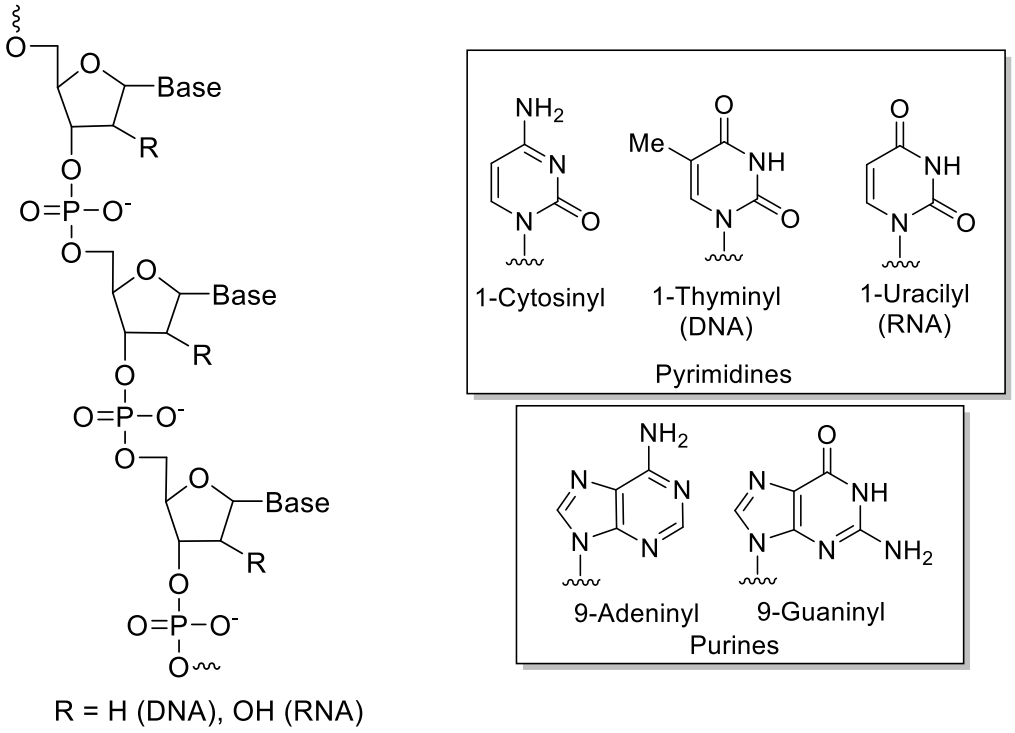

Figure 1: General structures of DNA and RNA polynucleotides and the bases.

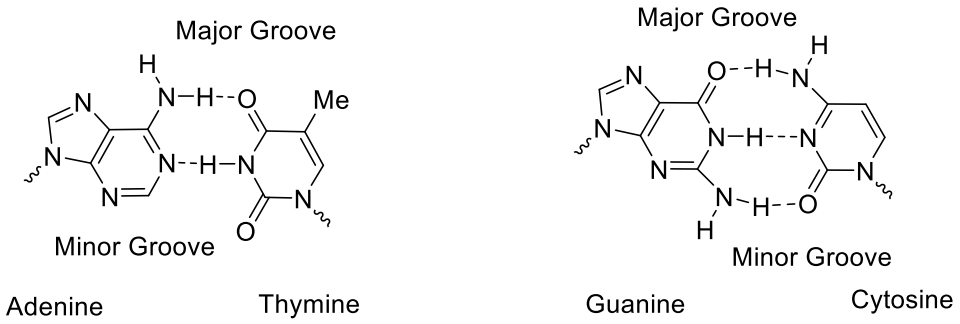

Figure 2: Interaction between the DNA bases.

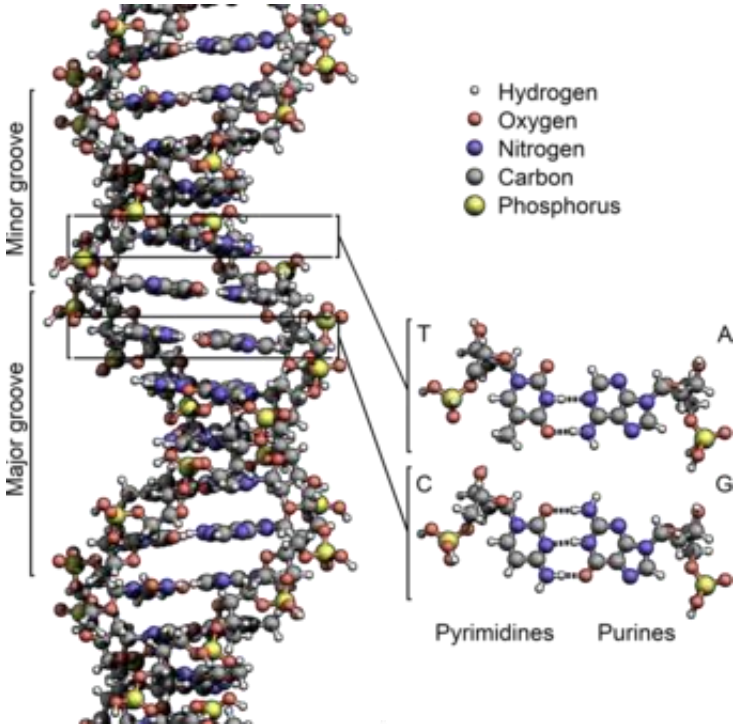

Figure 3: The double helix structure of DNA.[2]

In contrast to DNA, in RNA (ribose nucleic acid), uracil (U) replaces thymine and pairs with adenine. It also contains an additional OH group, making the formation of a double helix more sterically demanding. For both DNA and RNA, the stability of the double helical structure is enhanced by π-π interactions between the stacked planar hydrophobic aromatic rings of the adjacent bases on the polynucleotide chains.[3] This then exposes the anionic phosphate backbone of the DNA double helix (Figure 3) to the aqueous environment where the charge is neutralised by small cations such as Na^{+}, Ca^{2+} and Mg^{2+}, although it is also noted that there is large a hydration sphere which limits the strength of any electrostatic interaction.[4]

The AT and GC pairing which takes place between bases of two parallel DNA strands then gives rise to the secondary structure typified by the tertiary double helix structure. This can nominally adopt three different conformations: A, B and Z, (Figure 4) dependent on the primary sequence and other environmental factors such as hydration and ionic strength. [3] B-DNA is the most common form where the strands are held in a right handed anti-parallel double helix by stacking interactions between parallel oriented bases. The helix contains a major and minor groove, which differ in size, shape, hydration, electrostatic potential and the positions of the sites suitable

for additional hydrogen bonding.[5] The major groove has a width of ~22Å and the minor groove with a width of ~12Å. [6]

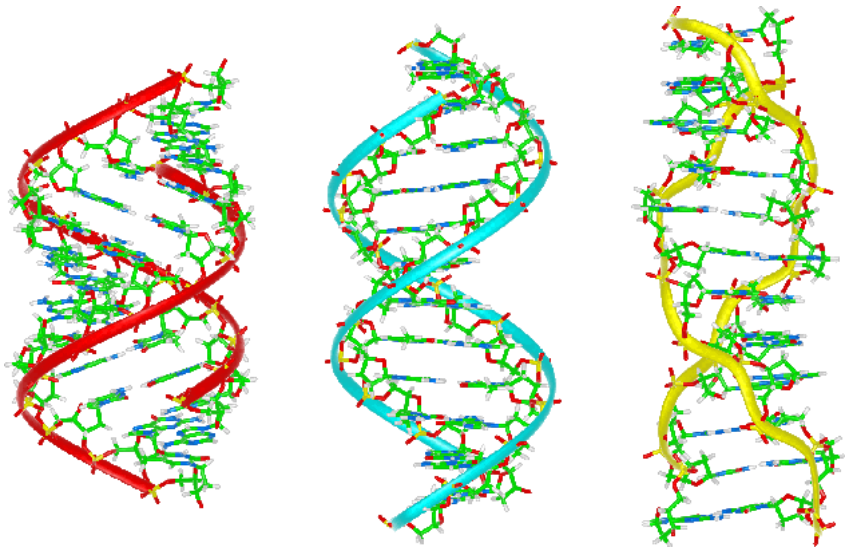

Figure 4 : The various conformations of double stranded DNA. A-DNA, B-DNA and Z-DNA.[7]

Due to the range of structural features available, and the number of accessible functional groups, DNA is a natural target for metal ion binding through a variety of identified “modes”, including direct coordination of the bases with the antitumour agents NAMI-A and cis-platin as discussed below.[8] DNA metal based interactions will of course depend on the identity of the metal ion, with simple hydrated ions such as Mg^{2+} and Zn^{2+} also functioning as cofactors in enzymatic reactions. The speciation and form of a transition metal complex can however, have significance by providing charge, a three dimensional structural profile, redox activity, possible photo-reactivity and an aptitude for site specific binding to the DNA macromolecule. [9]

Polar interactions with DNA within the grooves are very important in pairing stability and structure. The DNA bases themselves have hydrogen bond acceptors presenting in the minor groove that are normally well solvated. [10] These grooves therefore provide a space where potential and selective interactions can, and do, occur with metal ions, small molecules and complex ions. The major groove is a better candidate for sequence specific recognition by much larger entities such as proteins.[11]

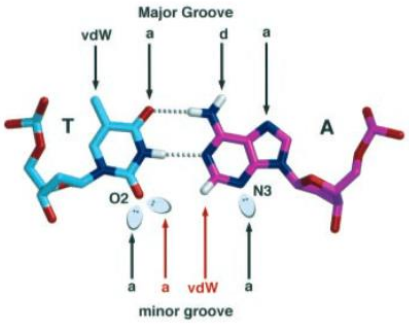

Figure 5: the structure of the major and minor groove in the TA base pair. Arrows indicate potential sites of discrimination for AT within the grooves. The ovals are the lone pair of electrons which are specific to the minor groove and Watson-Crick hydrogen bonds are indicated by the dotted lines. Potential recognition is labelled as: a for hydrogen bond acceptors, d for the hydrogen bond donors and vdW for van der Waals interactions. [11]

The minor groove is a target for the majority of non-covalent small molecular binding agents. The DNA binding with specific sequences, mostly with AT rich regions, typically takes place by a combination of hydrogen bonding to the base pair edges, van der Waals interactions with the minor groove walls, and electrostatic interactions. This can be the first step prior to alkylation or intercalation, which could be of interest as this could lead to antitumour activity. [12]

1.2 Modes of DNA Binding

Given the number of structural features within the secondary structure of DNA, “ligands”, i.e. small molecules that interact, are either typically neutral or cationic, and can undertake a range of different binding modes with DNA. Given the diversity and complexity in molecular structure and function, it is possible to present a three dimensional ligand structure which can have complementarity to the DNA and can lead to a number of identified different associations as highlighted below.

1.2.1 Electrostatic binding

Positively charged molecules can readily interact with the anionic DNA phosphate backbone, which releases the associated cations, e.g., Na^{+} and Mg^{2+}. [13] This reduces the electrostatic repulsion forces between negatively charged phosphate

groups and can contribute to the stability of the folded DNA conformation. The charge interactions depend on the salt concentration of the solution and the cations can show increased binding with DNA with decreasing salt concentrations. The ligands may also target the phosphate backbone through hydrogen-bonding interactions between the ligand and oxygen atoms of the phosphates.

1.2.2 Groove binding

Interactions within the grooves occur through non-covalent binding, where for example, the large concave cylindrical surfaces in the major groove interface with proteins. Whilst small molecules tend towards the minor groove and recognise the bases directly. This is usually sequence specific with the major groove showing greater shape variation with base sequences than the minor groove. [14]

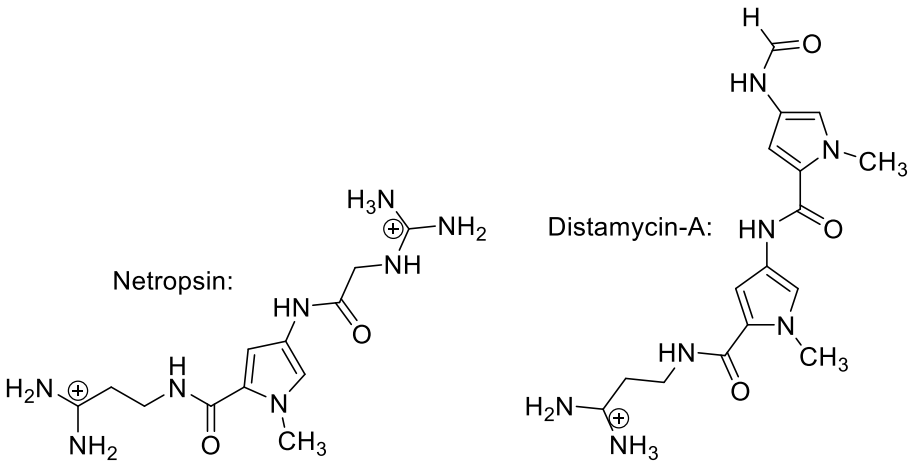

Figure 6: Structure of Distamycin A and Netropsin.[15]

An example of targeted minor groove binding includes the poly-pyrrole antibiotics Distamycin A and Netropsin (Figure 6).[15] Both these compounds are characterized by repeating pyrrole units connected by amide bonds ending with charged nitrogen atoms. They interact with the minor groove on the B form of DNA due to their curved shape which matches well with the structure of DNA. The deeper and narrower minor groove of AT rich sequences and the absence of the 2-amino group of guanine provides the optimum space to accommodate for the shape of the compound and to maximise the stability of van der Waals interactions. Hydrogen bonding between the base pairs in the grooves and the amide and electrostatic stabilizing interactions with the protonated amines are primary contributors to the overall DNA complex stability.

Distamycin has also been shown by NMR to bind to G-quadruplex DNA by intercalating between the terminal G-planes and the bases in the G-quartet structure.[15]

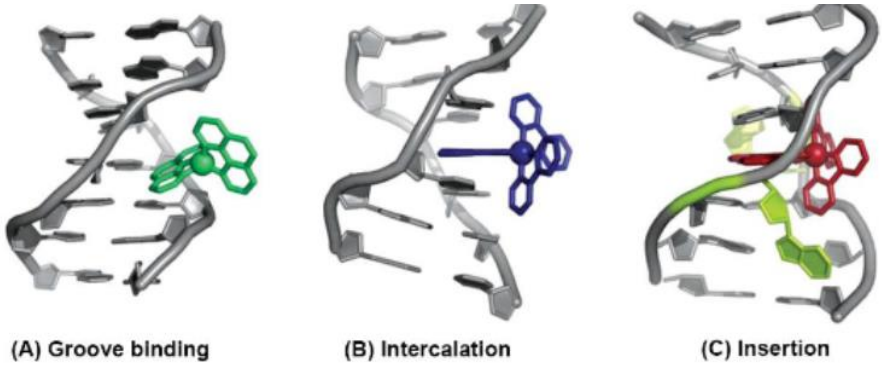

Figure 6: Three recognised binding modes of metal complexes with B-DNA.[16]

Metal complexes can also alter the orientation of the groove and displace the water molecules. Research on [Re(chrs)(CO)$_3$Br] (where chrs = 3-4H-chromen-4-one} (Figure 7) indicates that there are 3 absorbance maxima between 200 nm and 350 nm which are the intra-ligand π-π* transitions but the transition at 395 nm is due the ligand to metal charge transfer band (Figure 8). When adding CT-DNA to [Re(chrs)(CO)$_3$Br], hypochromism accompanied with bathochromism is associated with intercalation and involves a high π-π* stacking interaction.

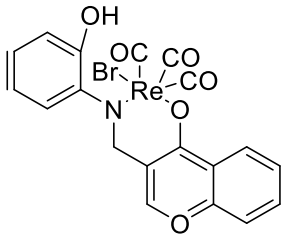

Figure 7: Structure of [Re(chrs)(CO)$_3$Br].[17]

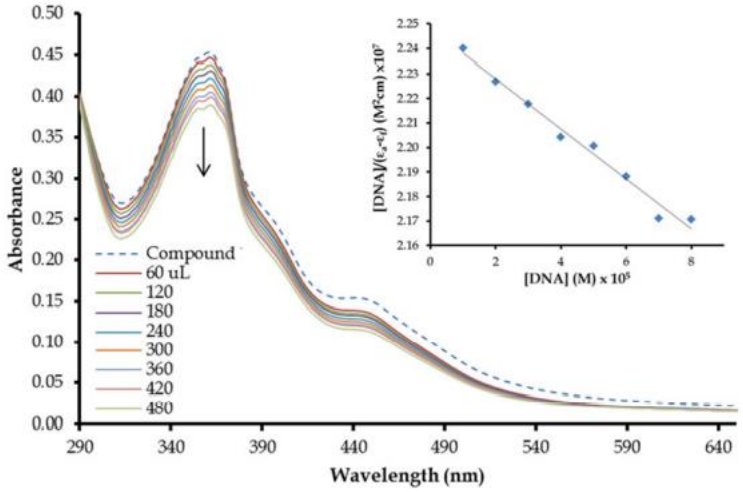

Figure 8: The UV-Vis absorption spectra. The dashed line indicates [Re(chrs)(CO)$_3$Br] free of any DNA and the hypochromic effect (indicated by the arrow) is due to progressive increments of CT-DNA (taken from ref 17 without permission).[17]

Molecular docking is a well established computational technique to predict the best interaction between a metal complex and DNA to form a new DNA-metal complex conjugate of the lowest possible energy. These results are consistent with groove binding due to the competitive polarity interactions breaching analogous interactions found within the interior and exterior of the CT-DNA double helix (Figure 9).

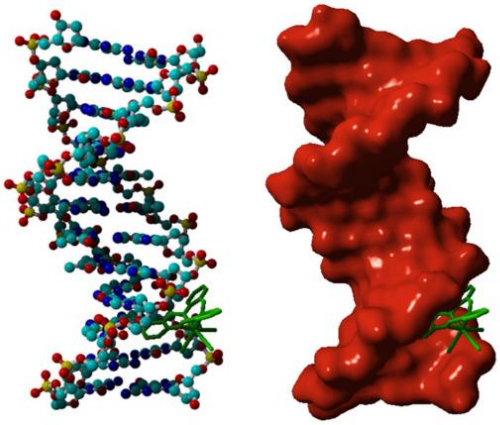

Figure 9: Binding to the minor groove of DNA. The structure on the left is the ball and stick model, and on the right is a molecular surface view (taken from ref 17 without permission).[17]

1.2.3 Intercalation

DNA intercalation occurs when an extended planar aromatic function, that could be appended to a transition metal complex, is inserted into the DNA strand between two adjacent base pairs to form sandwich like structures, either from the major, or the minor groove. Therefore, it opens a space between the base pairs and unwinds the helical twist a little. This affects biological processes like transcription, replication and repair, and for this reason it can be exploited in antitumour drugs and antiseptics. Due to their specificity for certain nucleic acid sequences, intercalators can also be used as stains for nucleic acids.[18] DNA intercalators are mostly polycyclic aromatic and planar compounds due to the strong pi-stacking interactions. An example of this is ellipticine (Figure 10) reported by Reha *et al*., which is a natural plant product which exhibits anti tumour and anti HIV properties. There was found to be an intercalation stacked above one DNA base pair.[18]

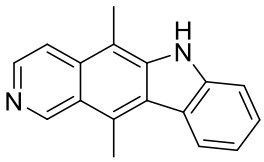

Figure 10: Structure of ellipticine.

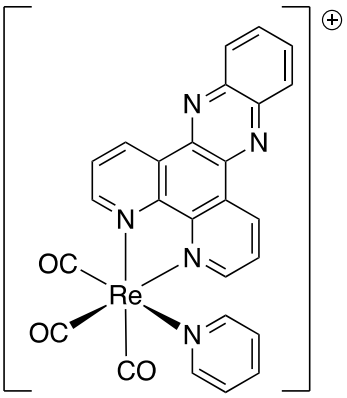

Figurę 11: $[Re(CO)_3(py)(dppz)]^+$ [19]

The Schanze group has reported intercalative binding of $[Re(CO)_3(py)(dppz)]^+$ (where dppz is dipyrido[3,2-a:2',3'-c]phenazine, Figure 11). The emission and absorption studies showed that the lowest lying excited state of the complex is not the expected MLCT, but a weakly phosphorescent dppz based intra-ligand triplet state.[19] UV-Vis spectroscopy showed a moderately intense band with the two maxima being at 366 and 384 nm which indicates the dπ(Re)→π* and the π→π*

transitions. They both also showed a DNA light switch effect, meaning that there was an emission enhancement on binding to DNA. The binding affinities with CT-DNA (K_b) are 4 – 5 x 10^4 M^{-1}, which implies that there is a modest interaction. This indicates that this monovalent complex is interacting with generic DNA through an intercalation interaction and that an electrostatic contribution is important as the stability constants are around two orders of magnitude lower than seen with other dicationic octahedral complexes containing the dppz motif.

1.2.4 Insertion

A number of larger compounds, often containing a metal complex, can take intercalation beyond extending a planar aromatic ligand into the base-stack to chemically corrupt the structure of DNA. Metalloinsertors eject the bases of a single base pair in a mismatch site with their planar ligand acting as a π stacking replacement in the DNA base stack.[20] This tends to occur where the DNA has been weakened through base pair mismatches. These may be from failed proof reading of replication polymerases or various exogenous agents like genotoxic chemicals or ionizing radiation. In healthy cells this is recognized and corrected by mismatch repair machinery. In some types of cancer the mutations in the proteins leads to an inactivation therefore the cancer cells have an abundance of DNA mismatched base pairs compared to healthy cells which makes mismatches a biomarker for cancer therapy. The first reported metal insertor was the complex $[Rh(bpy)_2(chrysi)]Cl_3$ (where chrysi is 5,6-chrysenequinone diamine; (Figure 10) which was shown to insert into DNA at the mismatched sites from the minor groove side, and ejects the mismatched bases and π-stack with the well matched DNA base pairs. The process is enantioselective, it is the right handed (D-complex) that binds to DNA.[20] The complex demonstrated high selectivity in killing tumour cells, with the behaviour attributed to the sterically expansive bidentate aromatic ligand which is too bulky to intercalate easily between the base pairs.

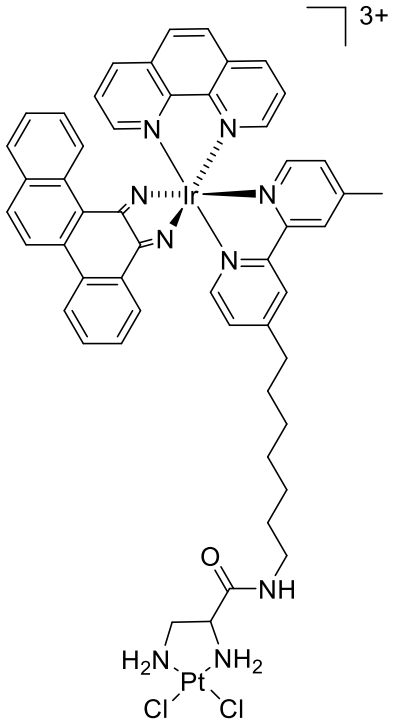

Figure 10: Structure of $[Rh(bpy)_2(chrysi)]Cl_3$ (where chrysi is 5,6-chrysenequinone diamine).[20]

1.3 Transition metals binding to DNA

The interaction of transition metal complexes with DNA has been used for cancer research and treatment with a variety of platinum containing agents over many years. This interaction can be either covalently (irreversible binding) or non-covalently (reversible binding). Covalent bonding occurs between the metal ion and the donor atoms of the DNA molecules by the loss of a labile co-ligand in the coordination sphere of the metal complex, followed by coordination of the metal centre to a nitrogen donor of a DNA nucleotide base. For example, the antitumour drug cisplatin, which has been used since the end of the 1970s as a chemotherapeutic agent in the treatment of testicular and ovarian cancers as well as bladder, cervical, head, neck and small cell lung cancers.[20]

The binding of metals to DNA has a few potential coordination binding sites. Binding to the oxygen atoms in DNA, such as the free hydroxyl groups in the sugars, or the phosphate groups, is known however this is rare with transition metals. There is however a high affinity of metals to coordinate to the N7 of the purines (A & G) as these are the most electron dense donors, accessible in DNA. They are exposed in

the major groove of the double helix and they are not involved in base pair hydrogen bonding.[20]

As highlighted above, non-covalent interactions between a complex and DNA can include electrostatic attraction with the anionic phosphate backbone, hydrogen bonding, van der Waals forces and hydrophobic interactions. This leads to reversible binding with DNA by phosphodiester backbone binding, groove binding, and intercalation through a π-stacking between the conjugated chromophores of the metal complexes and the DNA nucleotide bases. Non-covalent groove binding interactions are normally through a van der Waals or hydrophobic, and hydrogen bonding interactions, in either the major or minor groove of the DNA double helix, where displacement of the hydration sphere is the driving force to a positive interaction. There are also electrostatic interactions that could occur by columbic forces between a cationic metal complex, and the negatively charged phosphate backbone of DNA. [20]

The determinations of the nature of a metal complex or DNA interaction, whether its intercalation or groove binding, is normally eluded through the use of a combination of analytical techniques. Electronic spectral changes are normally considered whilst increasing the amount of DNA present to determine the binding strength and mode between the complex and DNA. The absorption of the metal complex with increasing concentration of DNA may increase (hyperchromism), decrease (hypochromism) or cause a red shift in the absorption wavelength of a selected peak (bathochromism). The combination of hypochromism and bathochromism normally relates to intercalation of metal complexes in the DNA double helix and a strong $\pi \rightarrow \pi^*$ transition, between the aromatic chromophore present in the metal complex and the base pairs of DNA. Normally, groove binding is shown by hypochromism and a negligible shift in absorption maximum wavelength. And as stated previously, normally, smaller molecules interact with the DNA minor groove due to small steric interferences.

Two of the significant inert complexes based on the d^8 square planar and d^6 octahedral metal ions which have provided a central scaffold for many metal-based DNA binding agents and have been used for a variety of applications including

probes of electron transfer processes within DNA itself. Some early work by Lippard and co-workers found that monocationic square-planar Pt^{II} complexes with the terpyridyl (tpy) ligand (Figure 11) interacted with DNA through intercalation with the binding constant, K_b being 10^5 M^{-1}. [21] The Sigman group also found that $[Cu(phen)_2]^+$ (where phen is 1,10-phenanthroline) which is a d^{10} system and hence quite labile, interacted reversibly through the minor groove and became a synthetic DNA nuclease.[22]

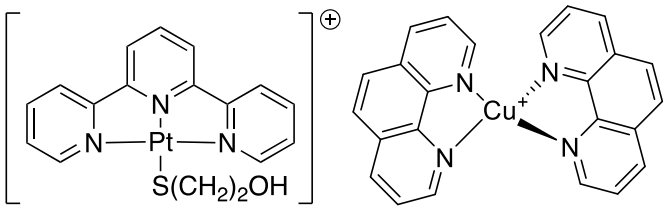

Figure 11: Pt^{II} terpyridyl and Cu phenanthroline. [21], [22]

In a study completed by Novakova and co-workers, where they studied a series of 4-chloropolypyridyl ruthenium complexes (Figure 13) in human tumour cell lines revealed that only the complex with three leaving chloride ligands, *mer*-$[Ru(terpy)Cl_3]$ displayed significant cytotoxicity.[23] This complex has the ability to form inter-strand crosslinks in the DNA which results in structural distortion in determining biological activities and not just the binding to DNA. *mer*-$[Ru(terpy)Cl_3]$ exhibited a slightly higher affinity to DNA 1.3 or 1.8 times higher than *cis*-$[R(bpy)_2Cl_2]$ or [Ru(terpy)(bpy)Cl]Cl respectively. The binding occurs preferentially at isolated guanine residues and results in conformational alterations in DNA by the unwinding the DNA helix. It is also shown that *mer*-$[Ru(terpy)Cl_3]$ shows a DNA inters-trand cross-linking in contrast to complexes B and C, which exhibits no such efficiency. Overall, this is covalently binding to DNA due to the higher oxidation states involved.

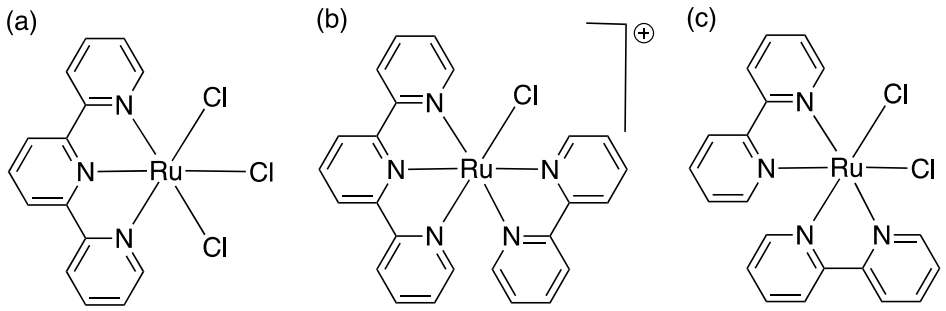

Figure 13: Novakova and coworkers investigation into DNA interstrand binding with (a) $[Ru(terpy)Cl_3]$, (b) $[Ru(terpy)(bpy)Cl]^+$ and (c) $[Ru(terpy)Cl_3]$.[23]

In a study completed by Tam and co-workers they investigated three inert ruthenium polypyridyl complex studies containing a beta-carboline ligand, and compared them to $[Ru(phen)_2(dppz)]^{2+}$ (Figure 14).[24] The b-carboline alkaloids (9H-pyrido[3,4-b]indole) (Figure 15) have been shown to have important pharmacological properties including anxiolytic, hypnotic, anticonvulsant, antitumour, antiviral, antiparasitic and antimicrobial activities, as well as being sedatives. It has also been shown to intercalate with DNA and for this reason they have been considered as anticancer drugs. The bulkiness and geometry of the coordinated b-carboline ligand may indicate that metalloinsertion plays more of a role in the binding interaction. With increasing concentrations of CT-DNA, hypochromism is shown at ~470 nm. With the emission spectra, when the concentrations of DNA is added, an increase is observed to 2.49, 2.97 and 7.48. So both the absorption and fluorescence studies indicate a strong interaction with DNA and the order of DNA binding affinity is 3>2>1.
Like $[Ru(phen)_2(dppz)]^{2+}$, they accumulate in the nucleus as well as the cytoplasm. But the complexes with the b-carboline ligands are more cytotoxic towards HeLa cells inducing apoptosis and autophagy. The cytotoxicities of the b-carboline complexes correlated well with their DNA binding affinities and the conclusion is that DNA may be their primary target *in cellulo*. This means that the activities of the complexes depend on more than just the binding affinities and potentially also on the cellular uptake and localisation.[24]

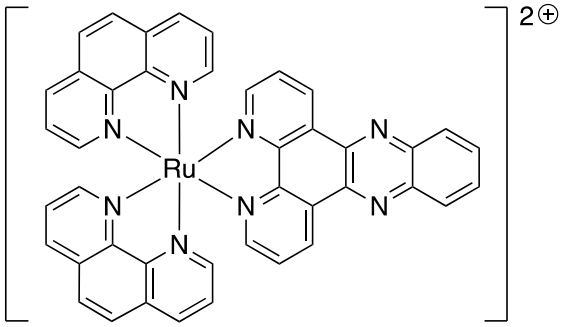

Figure 14: Illustration of $[Ru(phen)_2(dppz)]^{2+}$.

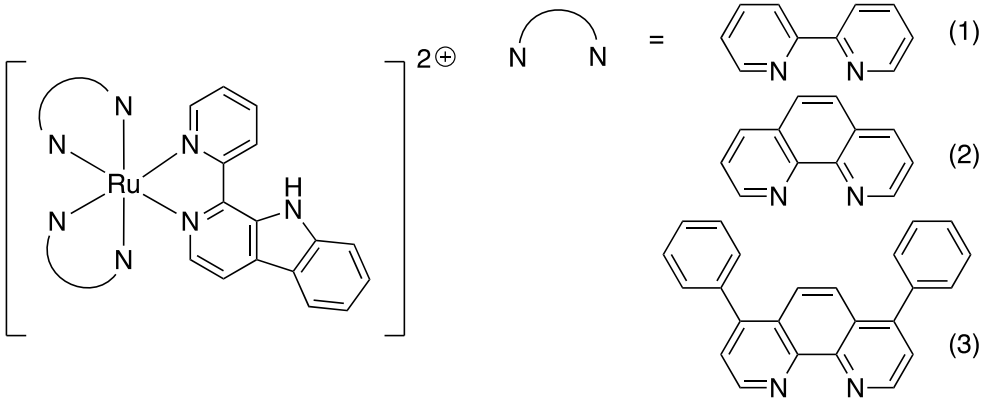

Figure 15: The b- carboline complexes studied by Tam *et al.* with (1) bipy, (2) phen and (3) dip co-ligands showing cell localisation in the cytoplasm and nucleus.[24]

1.4 Rhenium and Iridium Complexes and their Interaction with DNA

The metals used within this study include rhenium and iridium, where both these metals have been bound to DNA. Complexes of rhenium(I) and iridium(III) have received a lot of interest demonstrating an interaction with a number of biological molecules including DNA. This is because both cations can exhibit long-lived and intense MLCT emission in the visible region at room temperature upon photoexcitation with the correct ligand combination. Due to their environment sensitive emission, photoinduced electron transfer and photocatalytic properties, they have been extensively studied. Hence they can be used as biological probes and in cellular staining due to their intense and long lived emission, high cellular uptake efficacy and stability in aqueous solution. Both metal ions therefore can be considered for use as probes for ions, small molecules and biomolecules such as

DNA and proteins,[25] as intracellular sensors and bioimaging agents. They have high photostability, phosphorescence and a large stokes shift that can minimise self-quenching and be used to overcome the natural fluorescence present in many biological systems. Given the opportunity to tune the ligand structure, they can be tuned to offer cytotoxic activity, cellular uptake and bioimaging applications.
To date rhenium and iridium transition metal complexes have also been bound to organelles such as, the nucleus, golgi apparatus, nucleolus, mitochondria, [26] lysosome and endoplasmic reticulum. [27] Each organelle plays its own role to support the functions of the cell which means that organelle dysfunction can lead to variety of diseases such as, cancer,[28] Parkinson's,[27] Alzheimer's disease and diabetes.[26] This means that they can be a potential therapeutic target for a treatment of a variety of diseases.

There has also been two particular applications that have brought a lot of attention: oxygen sensing based on the long lived triplet states, and protein gel staining from the non-specific lipophilic interactions between the complexes and proteins. An example of this are the iridium acetylacetonate[29] complexes that have been used as oxygen sensors in living cells.

The luminescent tricarbonylrhenium(I) dimine complexes of the form $[Re(bpy\text{-}R^1)\text{-}(CO)_3(py\text{-}R^2)]^+$ and bis-cyclometalated iridium(III) species such as $[Ir(ppy\text{-}R^3)_2(bpy\text{-}R^4)]^+$ have been widely studied as biological reagents. Generally, they have large stokes shifts, long luminescence lifetimes and enhanced photostability. The tricarbonylrhenium(I) showed absorption and emission maximum at around 350 and 370 nm. It also shows good uptake into a variety of cell types. [30] Similarly to the bis-cyclometalated iridium(III) complex where these are taken up reasonably well by cells and show low cytotoxicity and for this reason they have been used as oxygen sensors in live cells. [31]

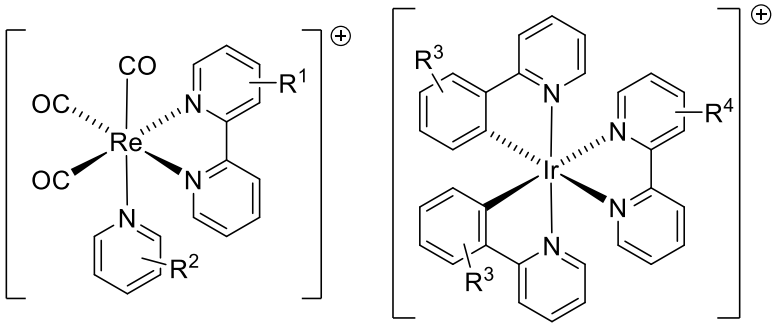

Figure 16: Tricarbonylrhenium(I) and bis-cyclometalated iridium(III) polypyridine complexes.[31]

Iridium(III) polypyridine complexes have also been used as dual emissive probes. These enable ratiometric sensing which offers more reliable detection of emission because the ratio of 2 emission intensities is measured instead of the intensity at one wavelength therefore interference by other parameters like the probe concentration can be minimized. One complex being $[Ir(ppy)_2(dpq\text{-}CONH\text{-}R)]^+$ (where R is biotin) where it binds to double stranded DNA providing a MLCT emission band at 602 nm, which is a typical feature of metallointercalators. Intercalation prevents quenching routes from the metal-stable excited π* levels and promotes MLCT emission.[32]

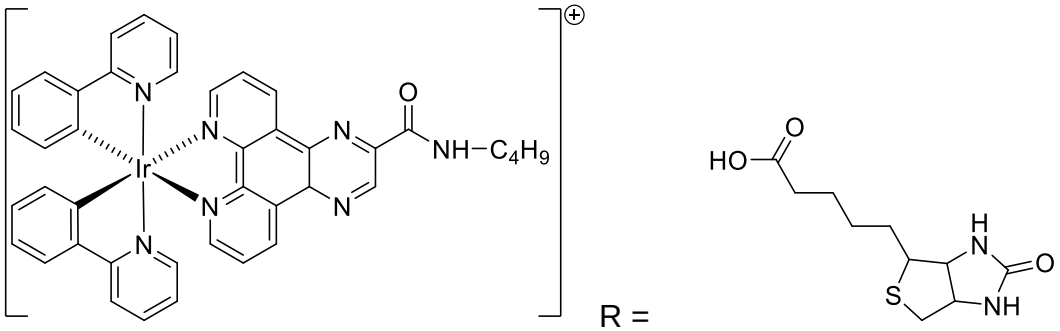

Figure 17: Structure of Ir(ppy)2(dpq-CONH-R)]+(R=biotin).

Cyclometalated iridium(III) complexes and the ligand 2,3-di(pyridine-2-yl)-pyrazino[2,3-f][1,10]phenanthroline (Figure 19), and the introduction of a small structural variation in the pyridyl ligand with DNA intercalation can be controlled, and these are “roadblocks” to DNA polymerase activity. When the concentration of the iridium complex increases a rapid polymerase chain reaction (PCR) based assay reveals this inhibition. Studying the inhibition of fundamental cellular processes can potentially offer an alternative route to cancer therapy. The UV-Vis and fluorescence properties in water and DMSO show that there is an overlap in the absorption and

emission spectra around 365 nm of the absorption of DNA and the iridium complexes. Circular dichroism (CD) spectroscopy can be used to show conformational change in biopolymers arising from a number of different external stimuli. This can include interactions with the metal complexes. In the case of B-DNA, there is a positive signal at ~270 nm which gradually decreases and a peak around 220 nm gradually increases. This shows a considerable interaction with DNA with the addition of the complex.[33]

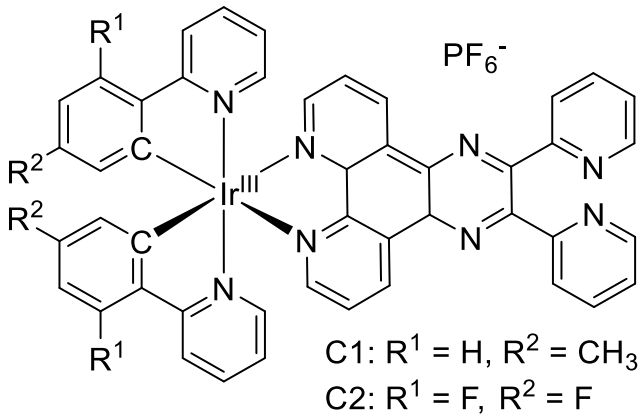

Figure 28: Structure of cyclometallated iridium(III) complexes with the ligand 2,3-di(pyridine-2-yl)-pyrazino[2,3-f][1,10]phenanthroline.[33]

1.5 Rhenium(I) Tricarbonyl Complexes

It has been shown that the general structure $[Re(CO)_3(dppz)(X)]$ where X could be a wide variety of axial ligands, are weakly emissive in aqueous media but shows an enhancement in the presence of DNA.[34] Rhenium tri-carbonyl complexes with bipyridines have been shown to be particularly useful for cell imaging experiments due to the flexibility arising from the additional coordination site. Generally a functionalised pyridine is used which controls cell uptake and localisation to the organelles such as, mitochondria, membranes, vacuoles and nucleoli. [34]

The rhenium tricarbonyl compounds normally show intense absorptions around 280 nm due to the ligand centered $\pi \rightarrow \pi^*$ transition and other weaker peaks and shoulders at around 380 nm assigned as the MLCT (metal to ligand charge transfer) $Re \rightarrow \pi^*$ absorption. Following intersystem crossing, a long lived triplet excite state can be formed, from which the luminescence is moderate, but when bound to DNA the intensity of the emission can increase as stated above.[34]

DNA binding reactions of $[Re(CO)_3(2\text{-appt})\text{-}Cl]$ (where 2-appt is 2-amino-4-phenylamino-6-(2-pyridyl)-1,3,5-triazine) (Figure 21) participates in hydrogen bonding and π-π interactions. On adding DNA, changes were observed in the absorption spectra (297-442 nm) with 5% hypochromism at 450 nm. This is an indication of intercalative binding. The complex is non-emissive in either “tris” buffer or acetonitrile so emission spectroscopy could not be used to examine the binding properties. With the DNA thermal denaturation studies, when compared to the untreated DNA (71^{o}C) though, the transition temperature increased to 83^{o}C in presence of the complex. And when increased to 90^{o}C, hyperchromism was observed with isosbestic points at 300 nm. [35]

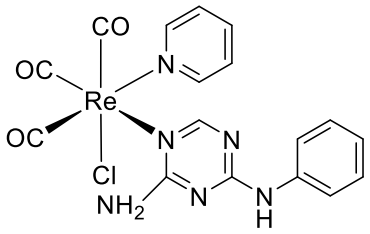

Figure 19: $[Re(CO)_3(2\text{-appt})\text{-}Cl]$, 2-appt being 2-amino-4-phenylamino-6-(2-pyridyl)-1,3,5-triazine.[35]

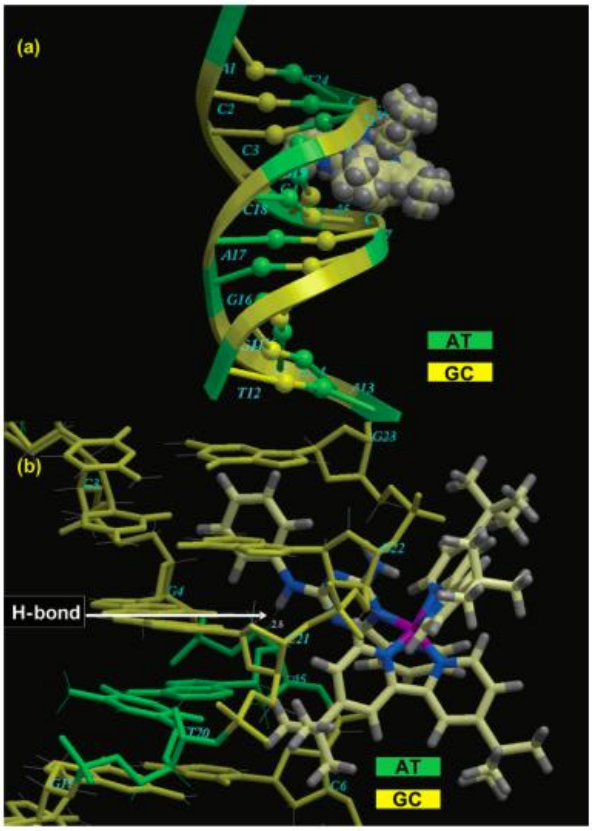

Figure 22:(a) molecular modelling of [Re(CO)3(2-appt)-Cl], with B-DNA (b) hydrogen bonding interaction with B-DNA, taken from ref 35 without permission.[35]

The conclusion is that the binding modes are at the AT rich regions of DNA. Binding with DNA showed hypochromism and insignificant shifts in the UV/vis absorption maxima, implying low binding constants which leads to the conclusion that it was bound via groove binding. The modelling study showed that the interaction was via the minor groove. [35]

1.6 Iridium(III) Polypyridine Complexes

Iridium complexes have been targeted for their use in biological imaging and diagnostics and have also been developed as imaging probes for specific organelles like mitochondria. The increased stability of iridium(III) complexes to ligand loss and the high degree of stereochemical control of the coordination environment in these complexes offers some advantages in in the development of DNA targeting systems. Cellular uptake is also related to hydrophobicity, and the low charge may be

advantageous for cell imaging therefore the synthesis has been carried out for a complex which contains a dppz and phenyltriazole ($C_9H_7N_3$) based ligand. [36]

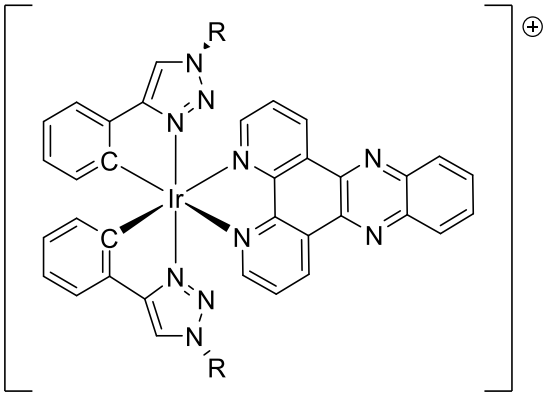

Figure 20: Structure of the iridium(III) complex $[Ir(ptz^R)_2(dppz)]^+$.[36]

The UV-Vis spectrum of the complex (Figure 21) shows an intense band in the ultraviolet region at 280 nm due to the ligand π→π* transition. The less intense lower energy absorption from 300 to 420 nm is due to the MLCT/LLCT transitions, however in this region there are further absorption bands due to the dppz ligand therefore there are additional LC contributions in this region. The complex was emissive in acetonitrile solutions and shows broad bands which indicates a long lived ^{3}MLCT/LLCT state around 672-675 nm which suggests that the photophysics are independent to the triazone substituent. This was initially carried out in dichloromethane and the emission maxima was 632 nm which blue shifted in comparison to the acetonitrile spectra. When decreasing solvent polarity the blue shift indicates the MLCT character and with the addition of DNA showed hypochromicity in the low energy bands typical of a solvated complex as it moves into the more hydrophobic environment of a DNA helix. This indicates that there is an interaction between the extended aromatic system of the complex and stacked bases within the duplex as there is an increase in emission as DNA is added, as would be anticipated given the similarities in behaviour to the previously discussed complex $[Ru(phen)_2(dppz)]^{2+}$.[37]

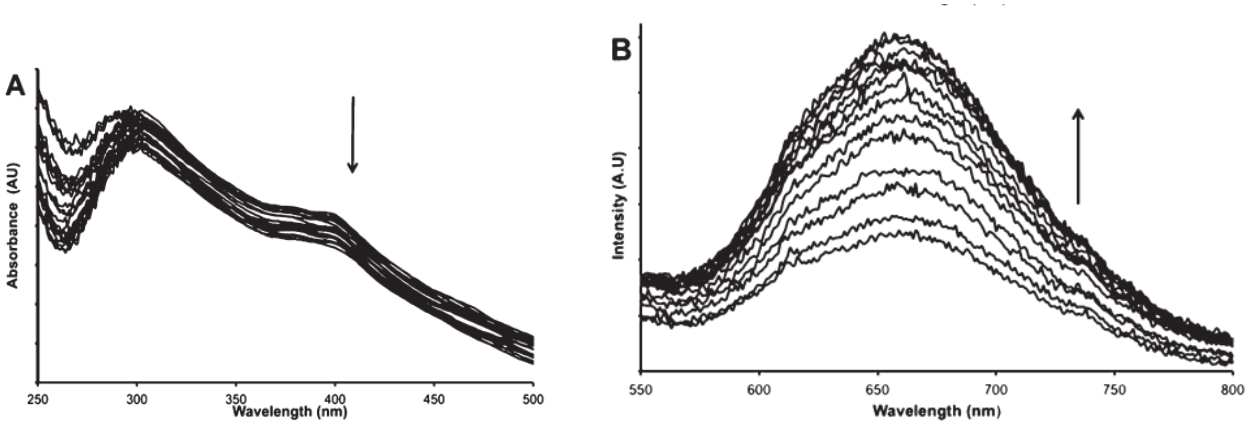

Figure 21: Emission and absorption spectra of $[Ir(ptz^R)_2(dppz)]^{+\cdot}$ (taken from ref 37 without permission).[37]

The cyclometalated iridium(III) complex $[Ir(tpyd)_2(2,9\text{-dmphen})]PF_6$ (where tpyd is 2-(*m*-tolyl)-pyridine; 2,9-dmphen is 2,9-dimethyl-1,10-phenanthroline) (Figure 22), did not provide significant changes upon the addition of DNA with regards to the luminescence. The blue shift at 17 nm in the emission maximum in the presence of DNA is indicative of increased hydrophobicity and rigidity of the local environment surrounding the G-quadruplex interaction over B-DNA. [38] In the interaction of luminescent iridium(III) transition metal complexes with DNA with emission studies, there is a large range of emission wavelengths as the iridium complexes can exhibit various emission colours depending on the electronic induction by the coordinated ligands.[38]

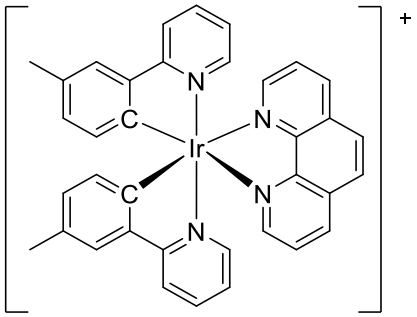

Figure 22: Chemical structure of cyclometalated iridium (III) complex.[38]

1.7 Pharmacological Activity of N-heterocycles.

Nitrogen containing heterocyclic derivatives have shown considerable pharmacological properties potentially arising from the similarities in structure to naturally occurring imidazoles such as histidine and adenine. [39] These have been explored with the thiazole and imidazole versions as they have various applications.

1.7.1 Benzimidazoles

Nitrogen containing heterocyclic derivatives have shown considerable pharmacological properties potentially arising from the similarities in structure to naturally occurring imidazoles such as histidine and adenine. [39] Benzimidazoles are a common feature in medicinal chemistry and new drug development. [40] The most prominent benzimidazole in nature is N-ribosyl-dimethylbenzimidazole which is an axial ligand for cobalt in the vitamin B12 core and benzimidazole derivatives are reported to be physiologically and pharmacologically active and are used in the treatment of several diseases including, epilepsy, diabetes and infertility. [40] For example, there was an investigation for the antimicrobial activity of the 2-substituted benzimidazoles (Figure 15) on six organisms: *Staphylococcus aureus*, *Proteus vulagris*, *Streptococcus faecalis*, *Klebsiella pneumonia*, *Pseudomonas aeruginosa* and *Escherichia coli* which can cause serious threat to the gastrointestinal tract in humans and animals. They were effective in most complexes, though screening the antibacterial activity using the well diffusion method.[40]

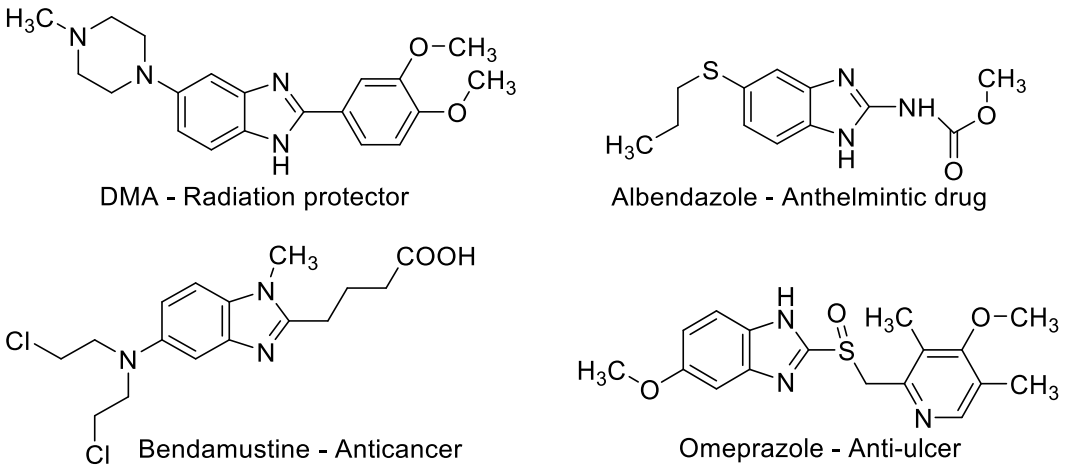

Figure 23: Pharmaceutically important and commonly marketed benzimidazole based drugs.[40]

1.7.2 Benzoxazoles

Structurally similar to benzimidazoles, benzoxazoles are used in research to evaluate new products that possess interesting biological activities like, antimicrobial, CNS (central nervous system) activities, antihyperglycemic potentiating activity, analgesic and anti-inflammatory activity.[41] They are also considered as structural isosteres of the nucleic acid bases adenine and guanine, which allows them to interact more easily with polymers of living systems.

Benzoxazoles have also been reported for use in various medicinal applications having shown, antidepressant, antibacterial, antifungal, anti-inflammatory, analgesic and anticancer activity. [41] An investigation was carried out by Kumar *et al.* who reported a bisbenzoxazole (which had been isolated from a strain of *Streptomyces*), showed efficacy against a range of human cancer cell lines including leukaemia, lymphoma and some solid tumour derived cell lines, with IC(50) values as low as 20 nM.[41]

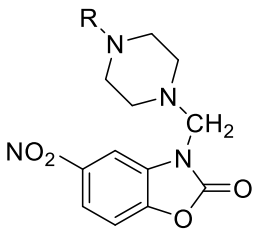

Figure 24: 5-Nitro-3-piperazinomethyl-2-benzoxazolinones – analgesic and anti inflammatory activity.[41]

1.7.3 Benzothiazoles

Similarly, benzothiazoles have shown antimicrobial, anticancer, anthelmintic and antidiabetic activities, and used in industry as antioxidants and radioactive imaging agents. An anti-bacterial study was carried out against *Escherichia coli*, *Pseudomona*s, *Serratia* and *Bacillus cereus* with the compound illustrated in figure 17 which showed high activity and moderate active against all strains. This was attributed to the presence of the thiazole and its indole heterocyclic ring systems. [42]

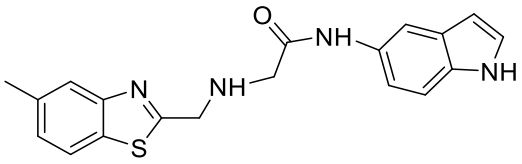

Figure 25: 2-((5-substitutedbenzo[d]thiazol-2-yl)methylamino)-N-(1H-indol-5-yl)acetamide.[42]

2 Aims

Rhenium and iridium bipyridine complexes have many great interests due to their ability of binding to DNA. Ruthenium(II) bipyridine complexes have previously been reported functionalised with benzothiazole, benzimidazole or benzoxazole groups (Figure 26). These were shown to bind to DNA potentially via the minor groove. The ligands proved to be very insoluble which meant that this hindered progress of the project. In particular, it was noted that these complexes precipitated out of aqueous solution in the presence of any phosphate salts including DNA itself. To overcome this difficiency it would be interesting to explore whether similar behaviour is exhibited when these ligands are bound to rhenium(I) and iridium(III), both of which are anticipted to have strong luminescence.

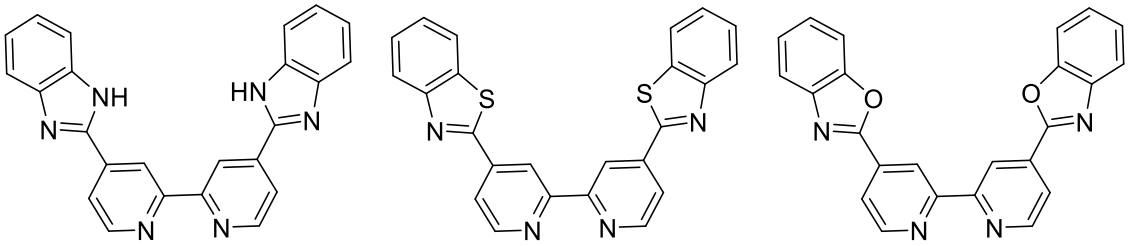

Figure 26: The BBOB (4,4'-bis(benzoxazol-2-yl)-2,2'-bipyridine), BBTB 4,4'-bis(benzothiazol-2-yl)-2,2'-bipyridine) and BBIB 4,4'-bis(benzimidazole-2-yl)-2,2'-bipyridine ligands that have previously been synthesized by the Fletcher group.

The principal objectives of this study are to isolate the rhenium tricarbonyl and iridium phenylpyridine analogous complexes to those shown in Figure 26, to explore their solubility and photophysical behaviour and to investigate whether they show any interaction with Calf thymus DNA, as a standard model for mammalian DNA.

3 Results and Discussion

3.1 Introduction

Within previous work in the Fletcher group, the BBOB (4,4'-bis(benzoxazol-2-yl)-2,2'-bipyridine), BBTB 4,4'-bis(benzothiazol-2-yl)-2,2'-bipyridine), and BBIB 4,4'-bis(benzimidazole-2-yl)-2,2'-bipyridine) ligands (Figure 27) have been synthesized. These have been bound to ruthenium(II) to form polypyridyl complexes, and their ability to interact with DNA investigated, where they have shown a potential interaction with the minor groove, especially where there is a broadening in the structures, such as those containing mis-matches or bulges sites. A difference in reactivity has been shown between the three different functional groups therefore we have utilised the oxazole, thiazole and imidazoles to indicate whether there is a difference between binding. To build upon previous work completed by the Fletcher group, we report here that these complexes have been bound to rhenium(I) and iridium(III) and preliminary DNA binding studies have been undertaken.

3.2 Synthesis and Characterization of Ligands

Initially the ligands had to be synthesised following on from previously reported procedures by Spillane [43] and Howells. [44] 4,4´-Dicarboxylic acid-2,2´-bipyridine was initially synthesized by the standard literature procedure by oxidation of 4,4´-dimethyl-2,2´-bipyridine with CrO_3.[45] This was then reacted with either 2-aminophenol, 1,2-phenylenediamine or 1,2-thiophenol dissolved in polyphosphoric acid and heated at around 150-200^{o}C for 16 hours (Figure 27). The reactions were cooled and poured into water. Saturated aqueous sodium carbonate was added to BBIB and BBOB and all three precipitates were collected by filtration, washed with water and dried. BBOB was surprisingly dark in colour, being almost black, whilst BBIB is dark green and BBTB is a light brown, giving the targeted products in a typical yield of between 49 to 65%.

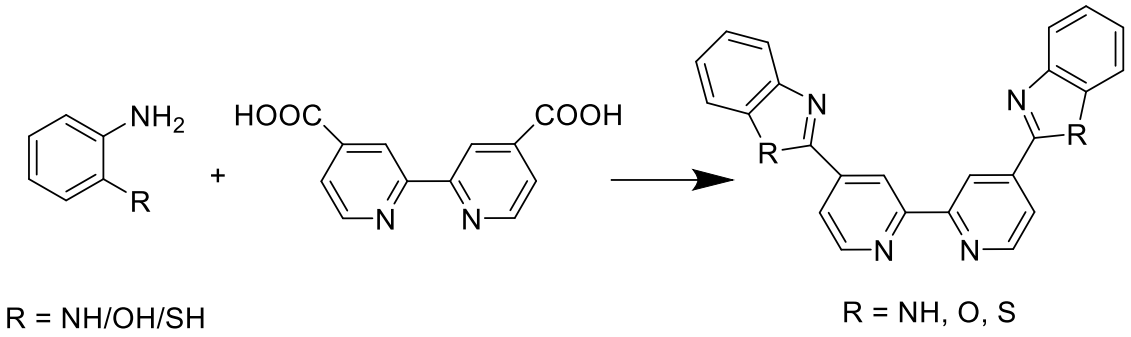

Figure 27: General synthesis of the ligands

The products all proved to be very insoluble in most common solvents, however sufficient material could be dissolved in warm DMSO-D_6 to permit characterisation by ^{1}H NMR spectroscopy (Figure 20,21,22) and the product confirmed by ESIMS with characteristic peaks for BBOB, BBIB and BBTB respectively. Unfortunately, due to solubility issues, ^{13}C NMR spectra could not be obtained, and it is assumed from the visual appearance, that the material could potentially be contaminated with co-precipitated phosphate salts.

^{1}H-NMR Characterisation:

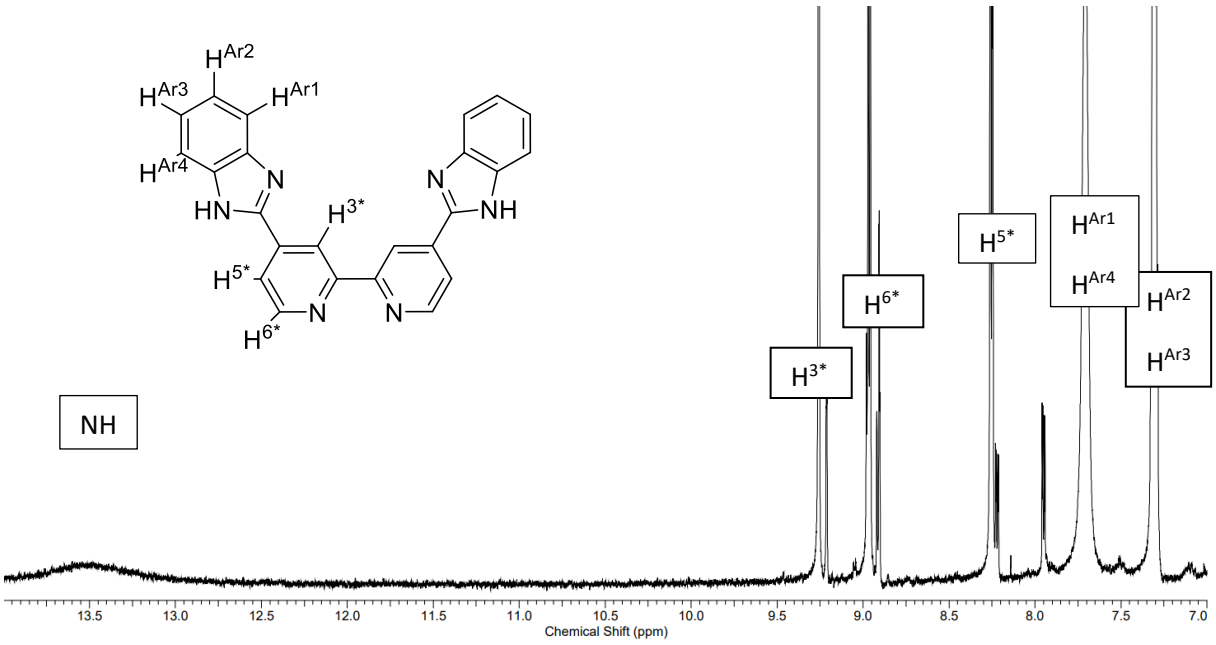

Figure 28: ^{1}H-NMR Assignment of BBIB in DMSO-D_6

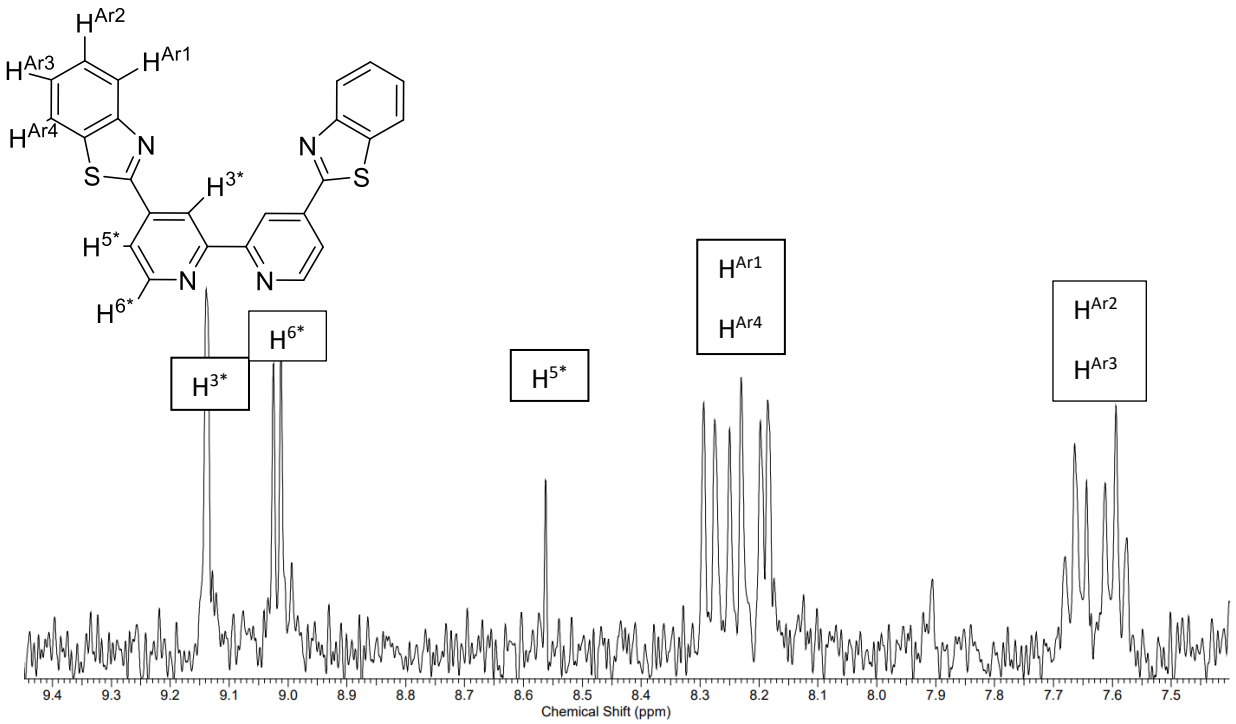

Figure 29: ^{1}H-NMR Assignment of BBTB in DMSO

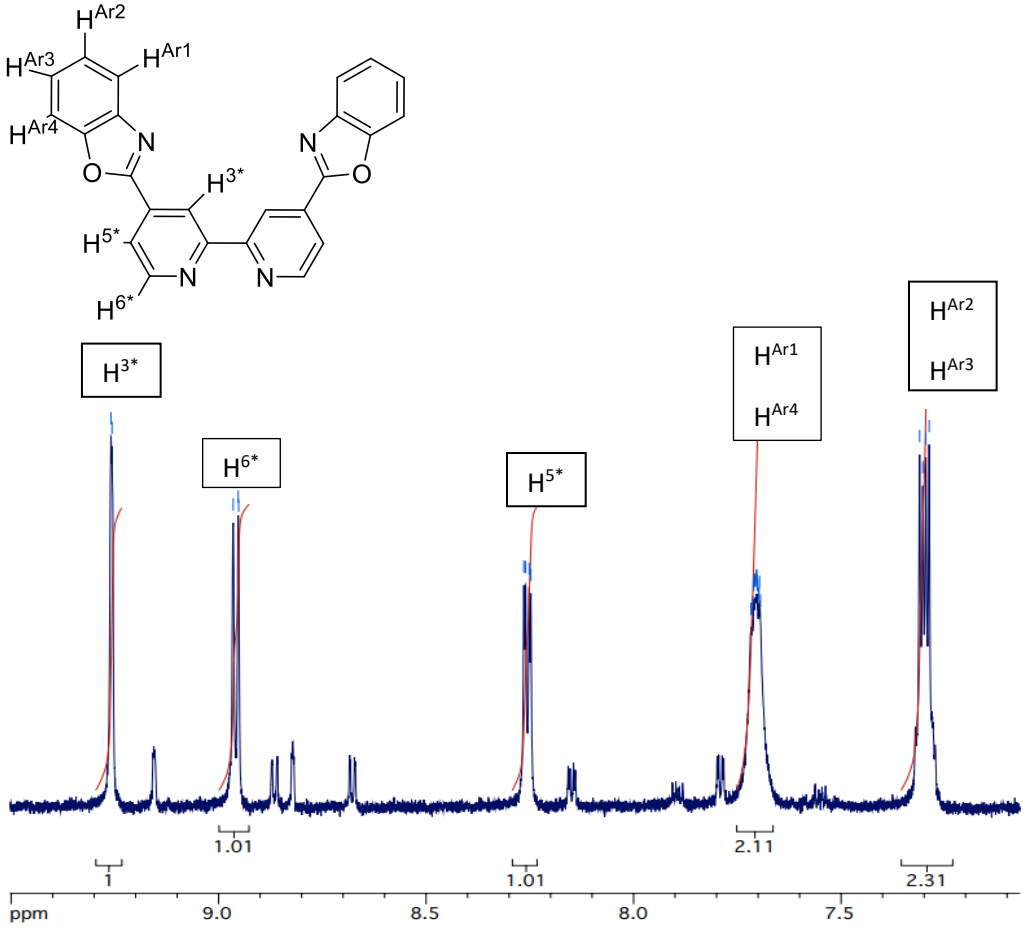

Figure 30: H-NMR Assignment of BBOB in DMSO-D_6

Each of the ligands were synthesized several times as some material was tentatively assigned as the “mono” functionalized within the NMR spectra following incomplete condensation on several occasions, particularly with the preparation of BBOB, with the possible presence of 4-benzoxazol-2-yl-4’-carboxylic acid-2,2-bipyridine. Attempts were unsuccessfully made to redissolve this intermediate in water to enable separation from the target product. But after several failed attempts it was realised that a slight excess of 2-aminophenol, 1,2-phenylenediamine, or 1,2-thiophenol, and heating the reaction mixture for a longer duration of time enabled the reaction to go to completion.

3.3 Synthesis of $[Re(CO)_3Br(L)]$

In theory, the synthesis of chelated rhenium polypyridines can be readily undertake by refluxing the ligand with $Re(CO)_5Br$ in toluene for a period of a few hours. [46] Unfortunately though the solubility of the three isolate ligands BBOB, BBTB and BBOB prevented this, and the partial dissolution in DMSO was exploited [47]. The synthesis of $[Re(CO)_3Br(L)]$ was completed by heating the respective ligand (BBOB, BBOB or BBIB), with $Re(CO)_5Br$ in DMSO at 120^{o}C for 16 hours. This formed a cloudy orange solution and once the resulting reaction was cooled, water was added which produced a very fine orange precipitate, which was isolated by filtration. This was a very slow process which took a few days with the fine powder either blocking the filter, or passing through it! In most cases the filtrate was effectively colourless, but in several instances the remaining solution was also orange, indicating that there could be other water soluble, potentially charged, species such as $[Re(CO)_3(L)(DMSO)]Br$ present. The yields obtained were: $[Re(CO)_3Br(BBOB)]$: 53%, $[Re(CO)_3Br(BBIB)]$: 50% , $[Re(CO)_3Br(BBTB)]$: 76%. The product resulting from this are also effectively insoluble in most common solvents and to enable ^{1}H NMR spectroscopy (Figure 21,22,23). The complex also had a bright orange fluorescence.

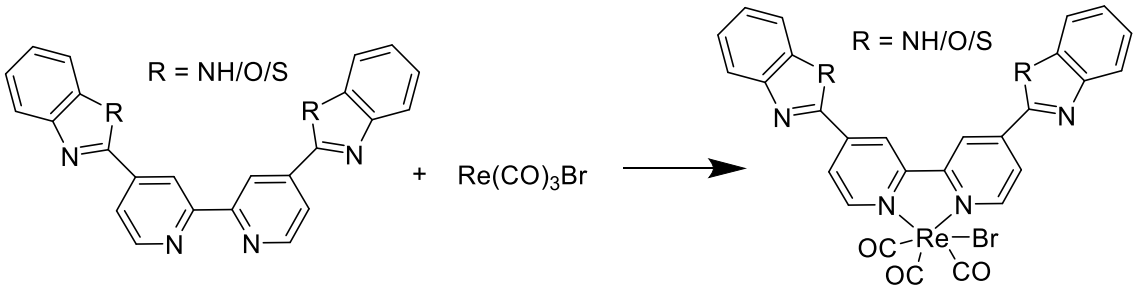

Figure 31: Reaction of $[Re(CO)_3Br(L)]$

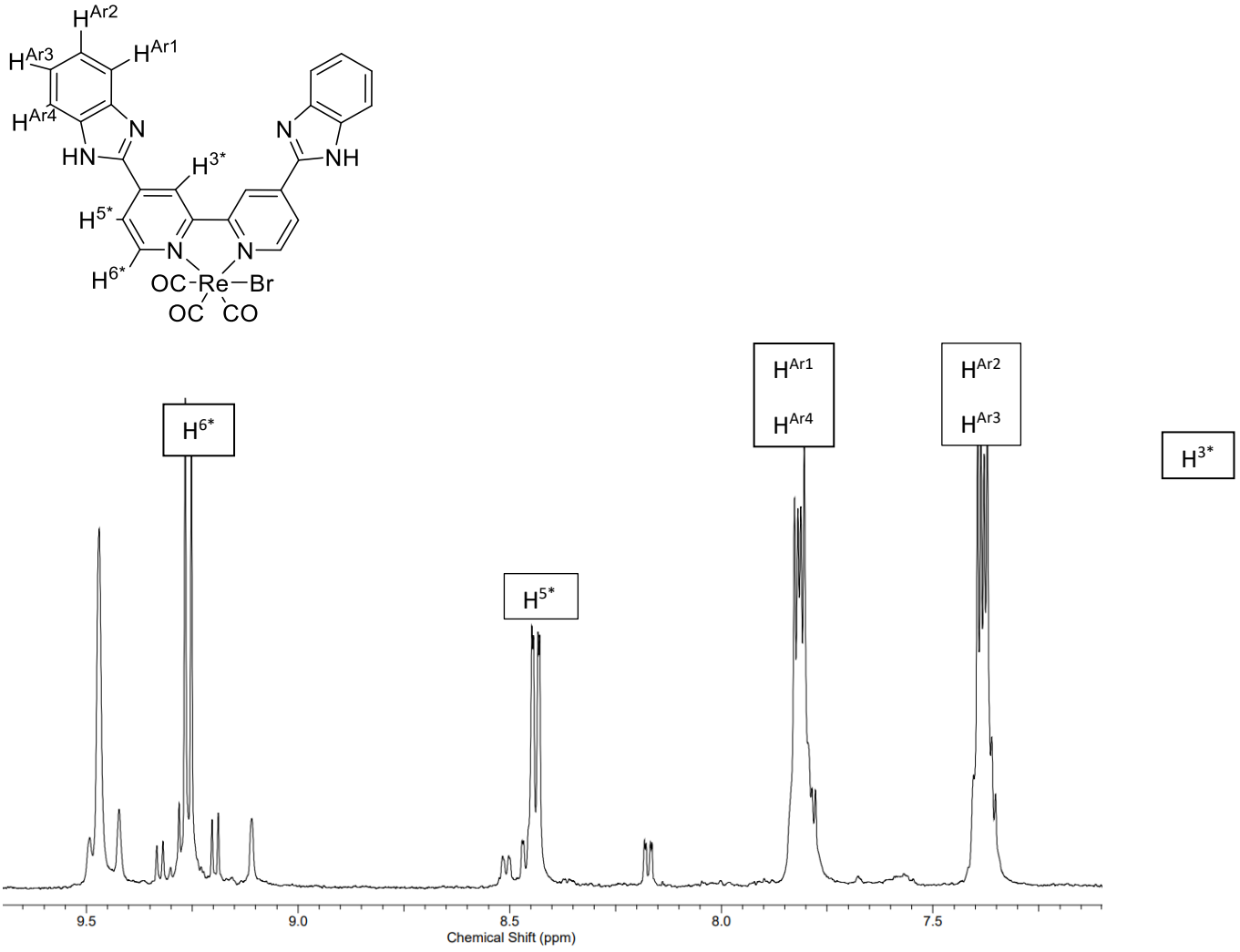

Figure 32: H-NMR Assignment of $[Re(CO)_3Br(BBIB)]$ in DMSO-D_6.

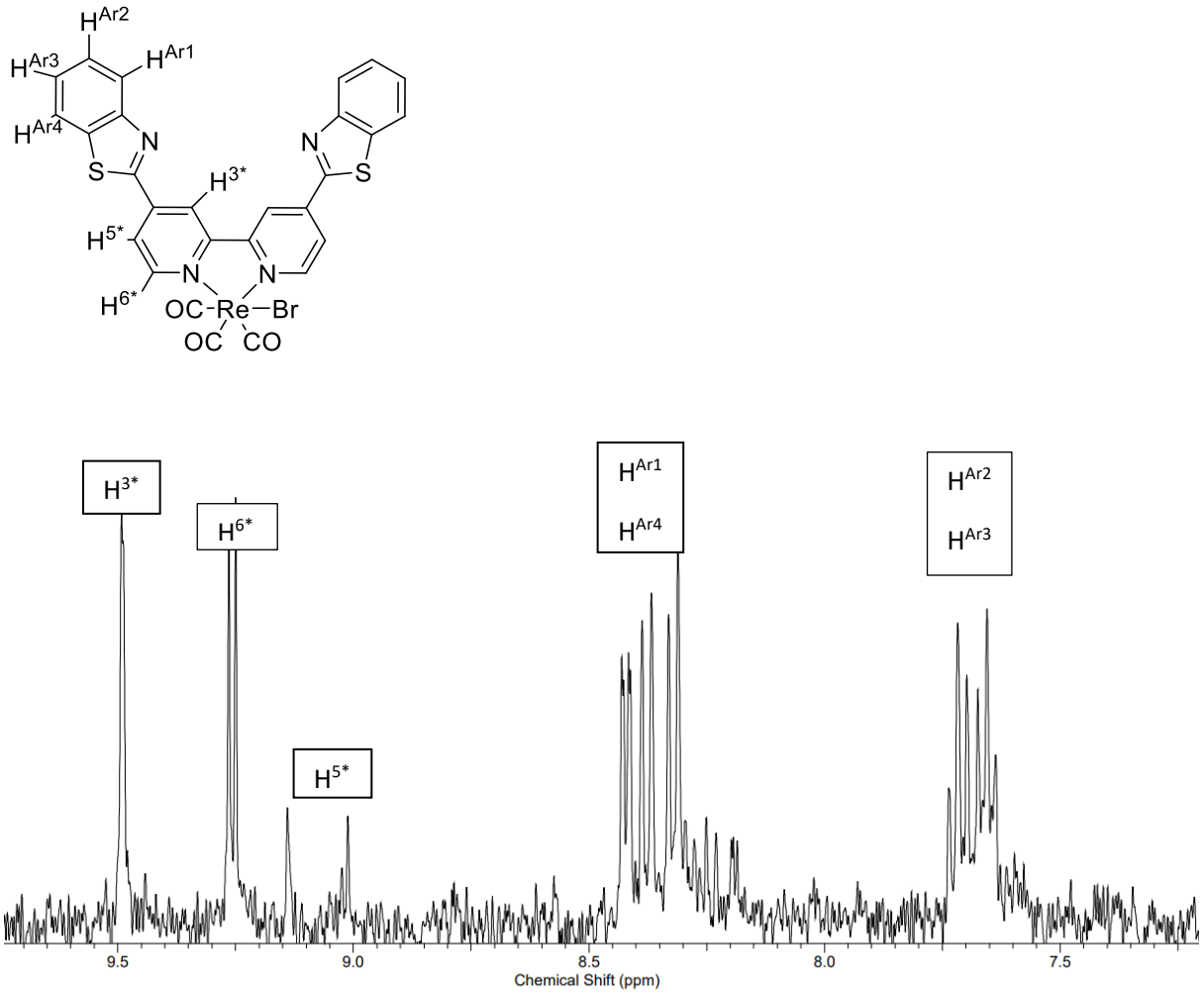

Figure 22: H-NMR Assignment of [$Re(CO)_3Br(BBTB)$] in DMSO-D_6.

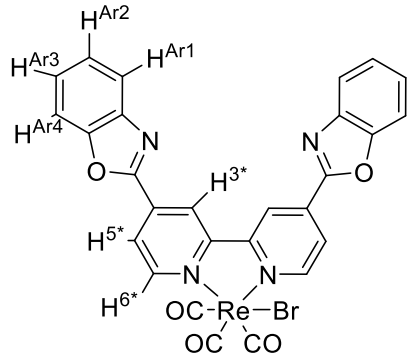

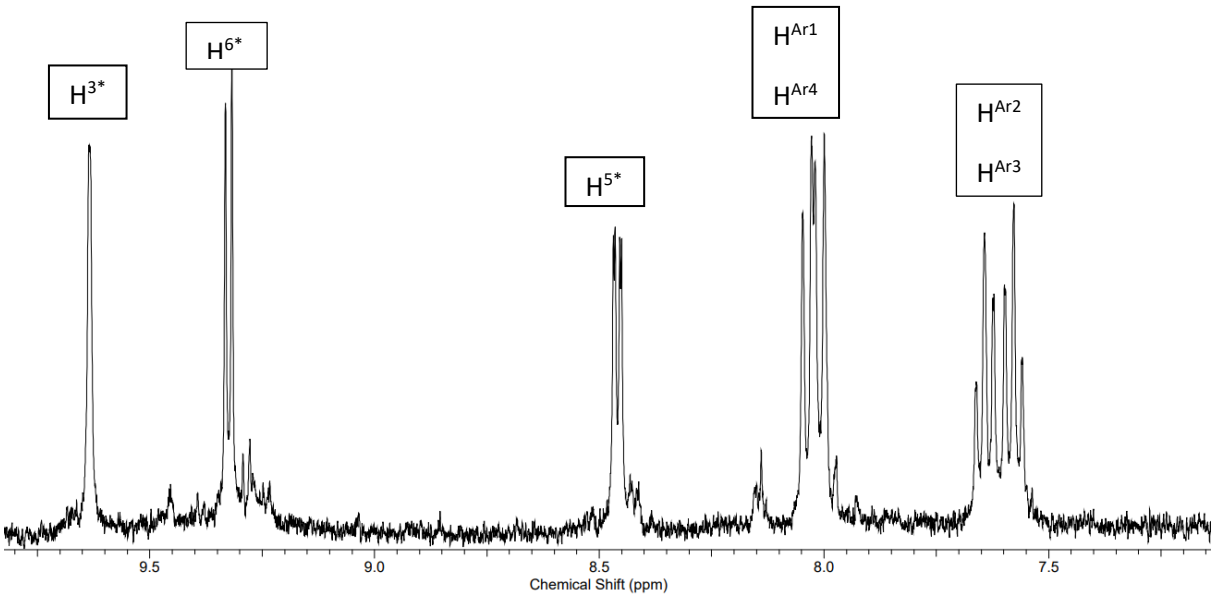

Figure 23: H-NMR Assignment of $[Re(CO)_3Br(BBOB)]$ in DMSO-D_6

3.4 Synthesis of $[Re(CO)_3Py(L)]BF_4/Cl$

In order to increase the solubility of $[Re(CO)_3Br(L)]$, (ideally in aqueous solution) a pyridine group was added to the three complexes to replace the bromo group. Initially this was attempted by $[Re(CO)_3Br(L)]$, pyridine and silver nitrate being heated at 120^{o}C for 3 hours. Tetrabutylammonium sodium chloride were added to remove the excess silver nitrate. It was precipitated from solution by the addition of water initially as the chloride salt and collected on Celite®. Following evaporation, the desired product was obtained as a yellow precipitate. The final product was then extracted with acetone, and dried given the product as a yellow powder. In the case of $[Re(CO)_3(BBIB)Py]^+$, the addition of water did not immediately result in precipitation, hence the complex was isolated by the addition of a small amount of $NaBF_4$.The yields obtained were: $[Re(CO)_3(BBOB)Py]Cl$: 37%, $[Re(CO)_3(BBIB)Py]BF_4$: 27%, $[Re(CO)_3(BBTB)Py]Cl$: 59%.

Characterization of the complexes in solution proved challenging. Initially the coordinated pyridine was evident in the NMR spectra, however on standing, it was observed that spectra rapidly deteriorated becoming broad and ill defined. The conclusion is that the pyridine ligand, unless in excess, was dissociating from the complex and was readily replaced by the solvent present, in the case of ^{1}H NMR

spectroscopy this was assumed to be the deuterated DMSO. Mass spectrometry data confirmed the identity of the complexes with a strong M^+ peak at 739.74 for amu for $[Re(CO)_3Py(BBOB)]^+$, although a peak at 701.80 amu assigned to $[Re(CO)_3ACN(BBOB)]$ indicated that the complex was undergoing ligand exchange when dissolved in acetonitrile prior to injection into the instrument. Similarly $[Re(CO)_3Py(BBTB)]^+$ gave peaks at 771.86 and 734.00 amu, whilst $[Re(CO)_3Py(BBIB)]^+$ could be detected at 738.12 as well as 700.00 amu.

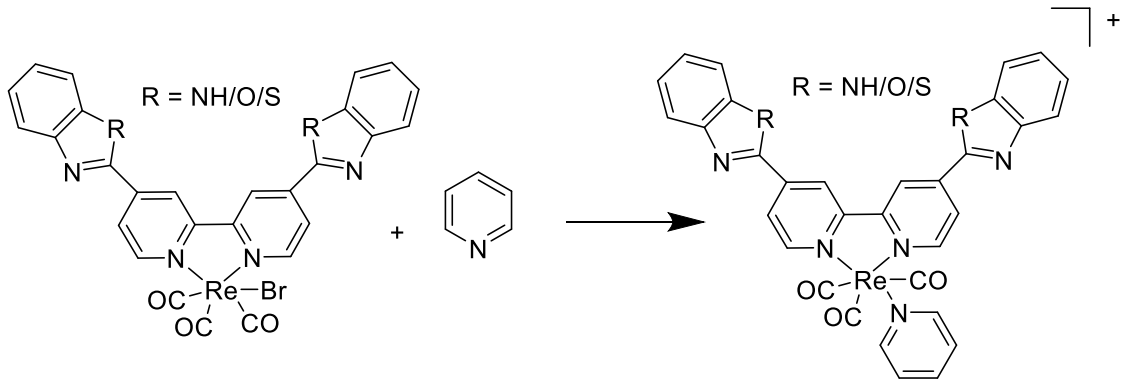

Figure 24: Reaction of $Re(CO)_3Py(L)]PF_6$

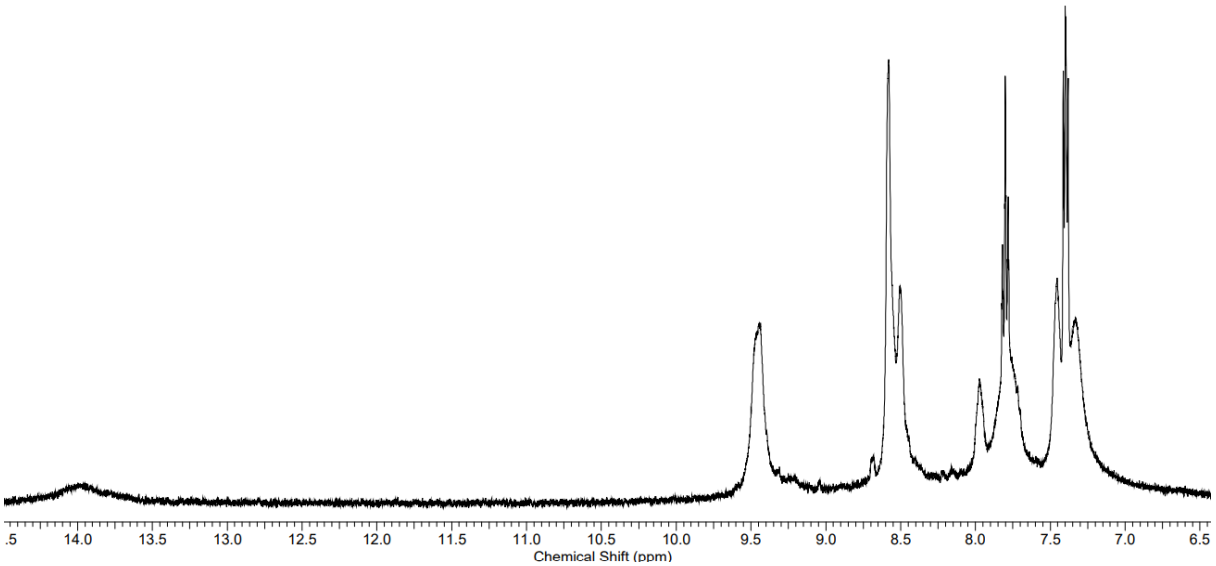

Figure 25: ^1H NMR characterisation for $[Re(CO)_3Py(BBIB)]BF_4$ in DMSO

The cationic complexes $[Re(CO)(L)(py)]^+$ all unfortunately had remarkably poor solubility in aqueous solution, even as the halide salts in tris-buffer, the environment required to explore the interaction with DNA. The only complex that was sufficiently soluble to investigate the DNA binding behaviour was $[Re(CO)_3(BBIB)Py]^+$ in mixture of tris buffer stabilised with DMF and methanol, although this precipitated on standing over a period of 48 hours, presumably arising from the exchange of the ligated pyridine with the excess of the chloride in solution. However this did permit some preliminary data to be obtained.

3.5 Synthesis of $[Re(CO)_3(L)T]^+$

Due to the solubility issues, after discussing this with Mike Coogan, he very kindly supplied us with *N*,*N*-bis(2-hydroxyethyl)-4-pyridinecarboxamide (T), where it as hoped that the hydroxyl groups would improve solubility in an aqueous environment. $[Re(CO)_3(L)T^+$ was prepared using $[Re(CO)_3Br(L)]$, acetonitrile and $AgBF_4$ under reflux to initially form $[Re(CO)_3(L)(ACN)]BF_4$ under nitrogen. This was then filtered using Celite® to remove any unreacted complex and silver salts. The acetonitrile was removed at reduced pressure on a Schlenk line. The remaining yellow solid, assumed to be $[Re(CO)_3Br(ACN)](BF)_4$, was then dissolved in dry THF (tetrahydrofuran) and N,N-bis(2-hydroxyethyl)-4-pyridinecarboxamide was then added and left to reflux for 3 hours. The THF was then removed under reduced pressure from the complex and this was dissolved in methanol and was then precipitated by a solution of KPF_6, the resulting product was a bright yellow solid. The products were then filtered using celite and removed using methanol. The yields obtained were: $[Re(CO)_3(BBOB)T]PF_6$: , $[Re(CO)_3(BBIB)T]PF_6$: 40%, $[Re(CO)_3(BBTB)T]$ PF_6: 44% This procedure did increase the solubility of the complex to allow DNA work to be completed, the solubility increased in methanol and acetonitrile.

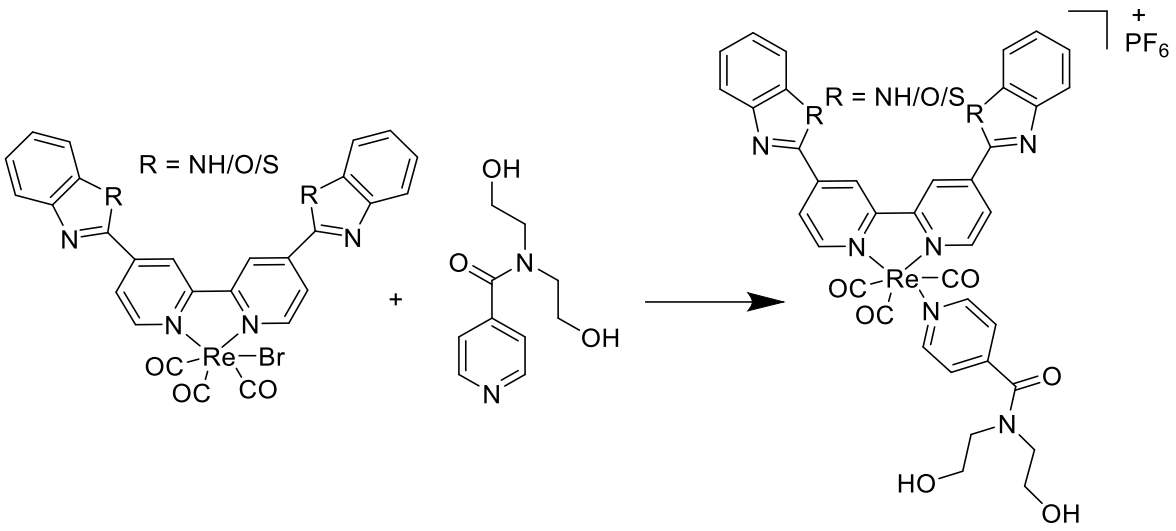

Figure 26: Reaction of $[Re(CO)_3T(L)]^+$

3.6 Photophysical Properties of $[Re(CO)_3Py(L)]^+$ and $[Re(CO)_3T(L)]^+$

All three complexes $[Re(CO)_3Py(L)]^+$ (where L = BBTB, BBOB and BBIB) show a similar absorbance and emission spectra (Table 1, Figure 27 and 28). For example, the complex $[Re(CO)_3Py(BBIB)]^+$, the absorbance spectrum (Figure 27) shows three observable peaks within the range of 250-600 nm. The band at 286 is assigned to the ligand π-→π* transition. The intense band at 336 nm and 383 nm can be assigned as the metal to ligand charge transfer (MLCT) d-→π* transition. And for all complexes, the emission spectrum (Figure 28) with an excitation wavelength at 420 nm, produced a strong emission around 600 nm.

Table 1. A summary the photophysical properties of $[Re(CO)_3(L)py]^+$.

	Absorption λ_{max} ± 1 nm	Emission λ_{max} ± 1 nm
$[Re(CO)_3(BBTB)T]^+$	290	130
	350	
	395 (sh)	
$[Re(CO)_3(BBIB)py]^+$	286	160

	344	
	391 (sh)	
$[Re(CO)_3(BBOB)T]^+$.	280	**100**
	325	
	371	

*The spectra of the complexes were recorded as their in acetonitrile at 298 K. λ_{ex} = 420 nm when absorption = 0.1.

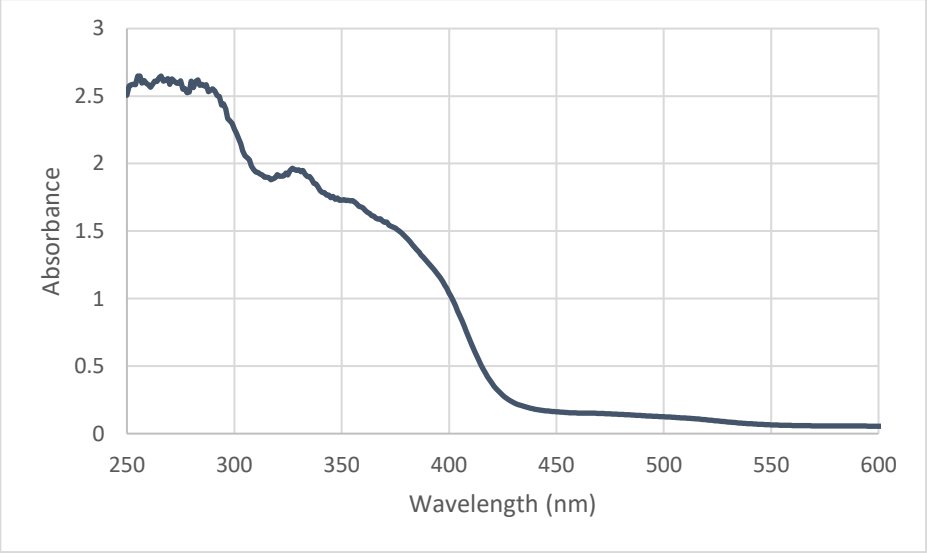

Figure 27: UV-Vis absorbance spectrum of $[Re(CO)_3Py(BBIB)]^+$ in acetonitrile

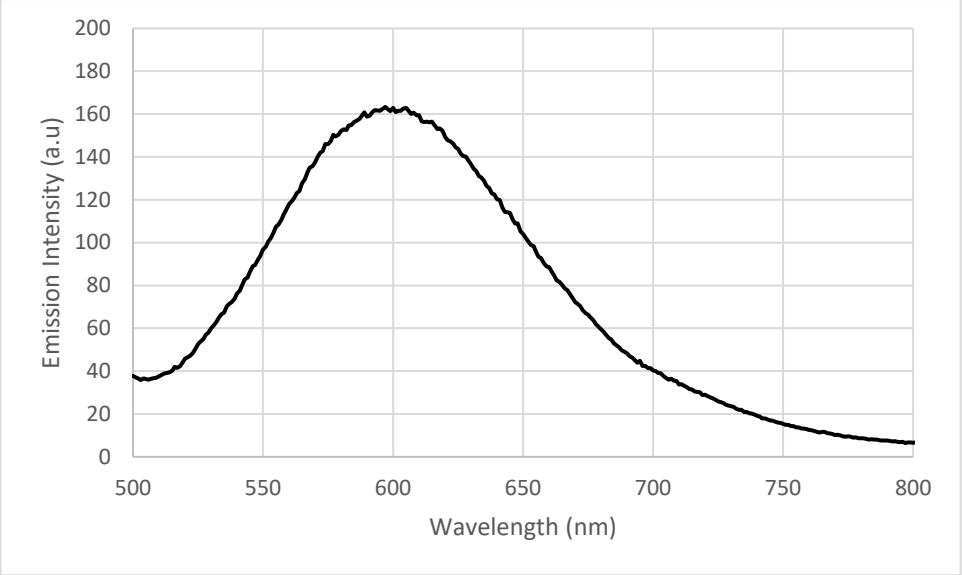

Figure 28: Emission spectrum of $[Re(CO)_3Py(BBIB)]^+$ in acetonitrile with excited at 420 nm.

3.7 UV-Vis absorption and Emission DNA Binding Studies of $[Re(CO)_3(BBIB)Py]^+$

UV-Vis for absorbance and emission studies can be used to determine the nature of binding to DNA with metal complexes. When an interaction occurs between DNA and a complex the photophysical properties can alter, which can potentially indicate the type of binding that has taken place. Both the rhenium complexes and DNA have strong absorbance peaks between 200 and 300 nm. But changes in the metal to ligand charge transfer (MLCT) can be monitored in the “complex only” region of the spectrum from 300 to 500 nm allowing for comparisons to be made between bound and unbound forms of the complex. A “light switch” effect, where the emission is enhanced can also occur when bound to DNA which normally occurs weakly with a groove binding complex, or more strongly when it experiences intercalation.

To investigate the behaviour of these complexes with DNA, attempts were made to dissolve the complex under investigation in aqueous “Tris” buffer solution to ensure that there was a stable pH and electrolyte environment for the DNA. It was however very difficult to get the rhenium complexes into aqueous solution. They would initially dissolve, or could be persuaded, into solution in a small quantity of DMSO, DMF, acetone, acetonitrile, or methanol, before adding the Tris buffer solution, but then over time they would precipitate out. Various solvent mixtures miscible with aqueous-

tris buffer solution were explored settling eventually on using 50% DMSO with 50% tris-buffer mixture.

Sadly, out of the three rhenium pyridine complexes $[Re(CO)_3Py(L)]^+$ (where L = BBTB, BBOB and BBIB), the only complex that was soluble enough to dissolve in tris buffer containing 50% DMSO, was $([Re(CO)_3(BBIB)Py]^+$, therefore only UV-Vis and emission studies in the presence of DNA were completed on this complex. With the analogous BBOB and BBTB complexes the materials proved too insoluble to complete studies. In reality, the complexes are likely to be dissociating the pyridine ligand, and in a buffer solution that contains a considerable amount of chloride ions, it is likely that the pyridine is being displaced initially by the solvent, and then the halide ion resulting in the neutral complex $([Re(CO)_3(BBIB)Cl]$, which precipitated.

The absorption and emission spectra were recorded for the solution of $[Re(CO)_3(BBIB)Py]^+$ (although we can assume this is likely to be $[[Re(CO)_3(BBIB)DMSO]^+$ predominantly) in the presence of increasing concentrations of DNA (Figure 29). Disappointingly, the absorbance spectra show very little change in the presence of DNA. This does not indicate that a binding is not occurring, just that it may be as a result of an ion pairing that does not affect the chromophores involved. The emission shows a slight increase upon the addition of DNA, however this is not the drastic changes that were found in the studies highlighted in Section 1.

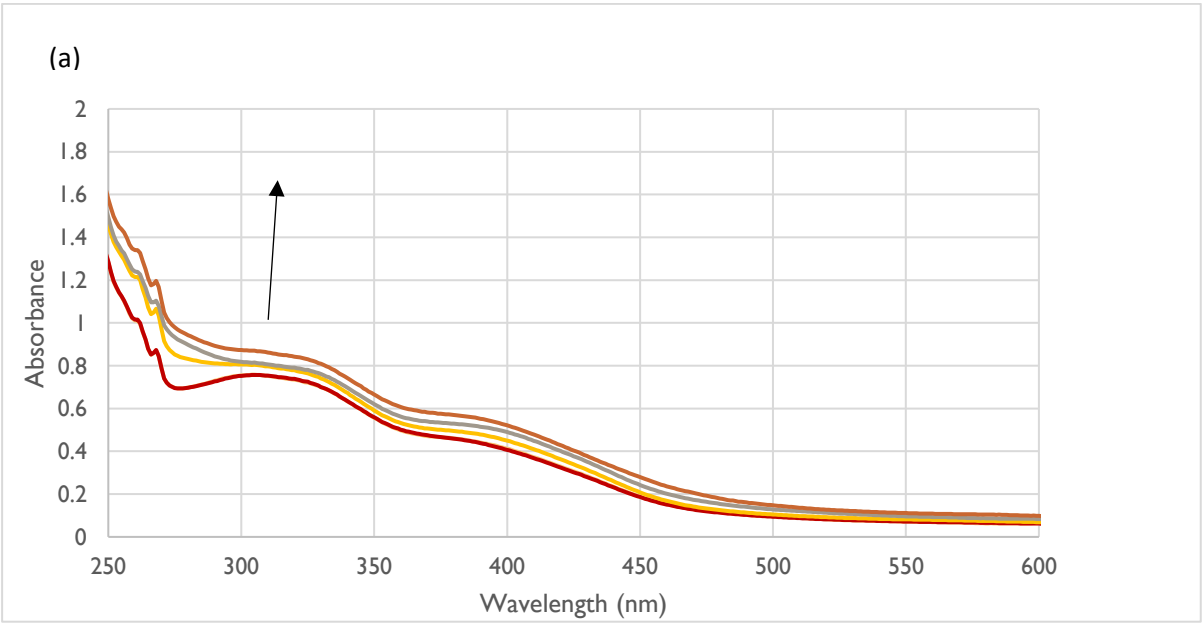

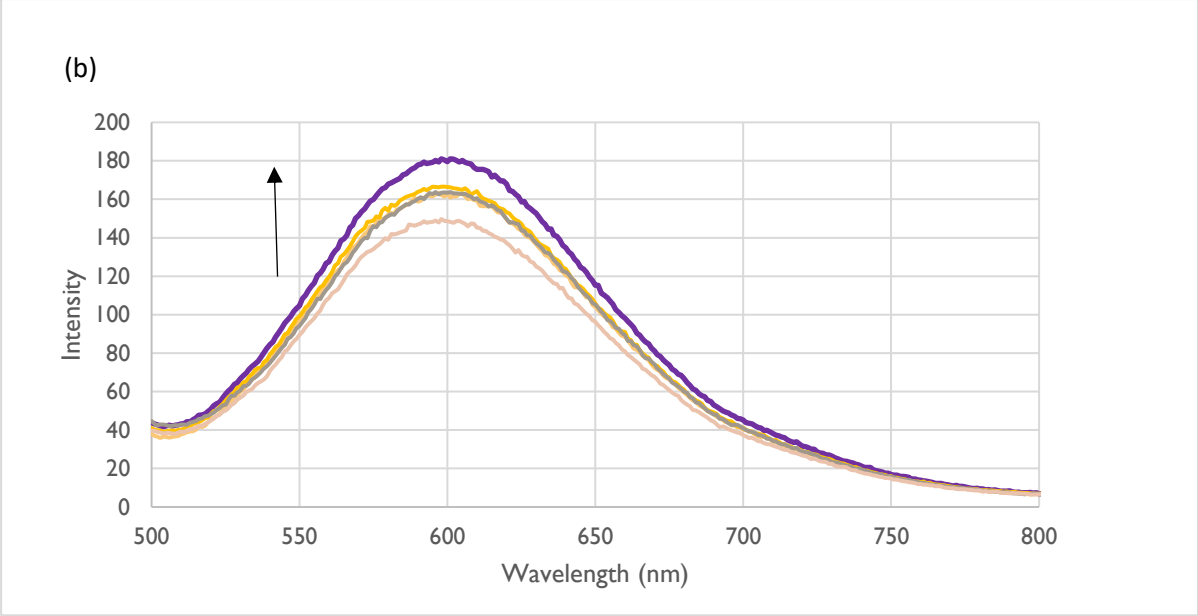

Figure 29: a) UV-Vis for the absorbance and b) fluorescence for the emission of $[Re(CO)_3(BBIB)Py]^+$ with increasing amounts of DNA in tris buffer, DMSO and acetonitrile solution.

The complexes $[Re(CO)_3T(L)]^+$ showed better initial solubility in Tris buffer but however like the analogous pyridine complexes on standing they too precipitated indicating ligand substitution reactions are likely to be occurring. In the presence of CT-DNA, similarly the absorbance spectra do not show any major changes, however as the amount of DNA is increased there is a small increase in the intensity of the emission, which would indicate that the local environment around complex is changing, with at least one of the quenching routes being inhibited consistent with the complex being weakly associated with the DNA. In order to establish a trend further emission and absorption studies will need to be carried out.

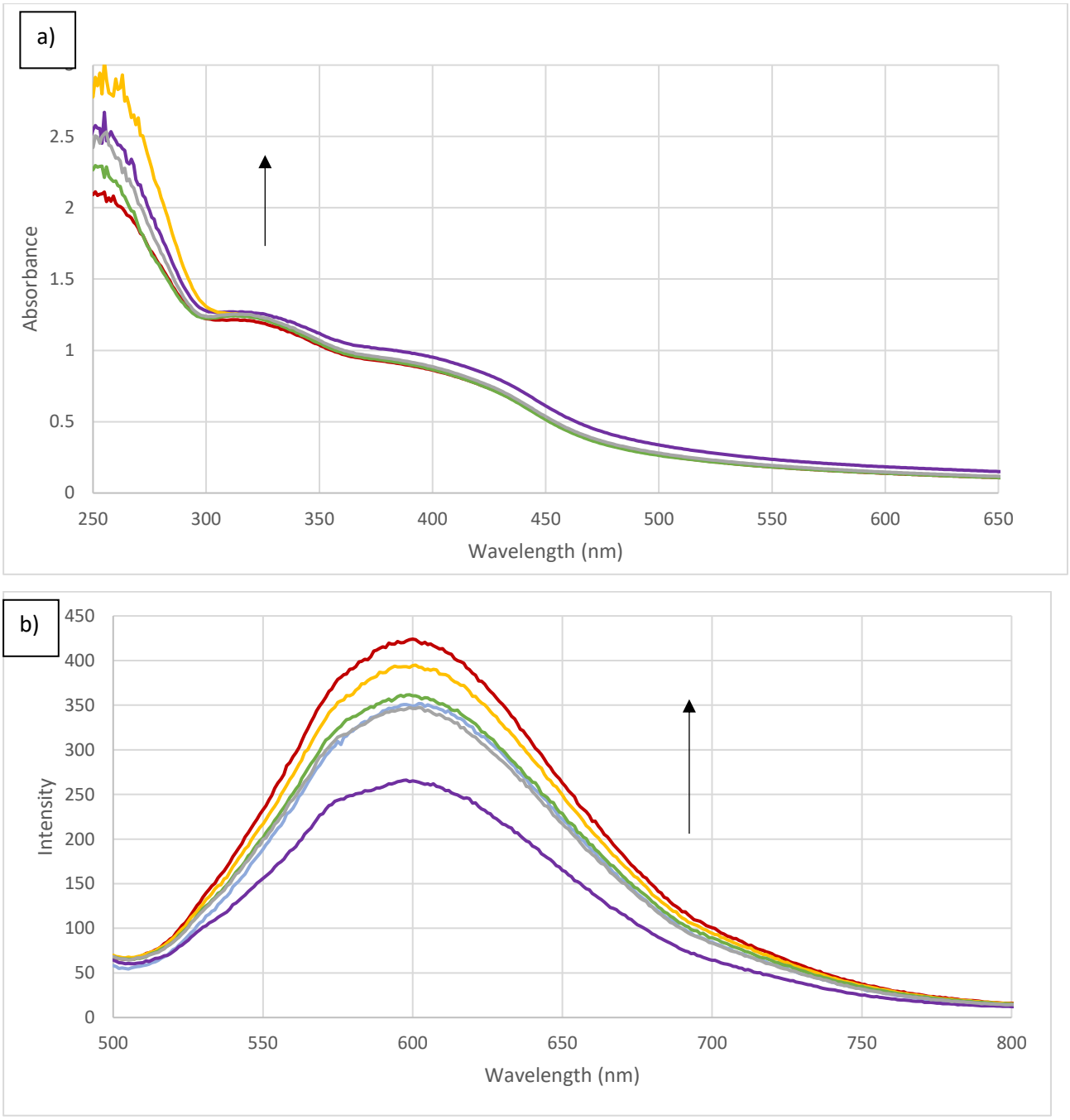

Figure 30: a) UV-Vis for the absorbance and b) fluorescence for the emission of $[Re(CO)_3(T)(BBTB)]$ with increasing amounts of DNA in tris buffer, DMSO and acetonitrile solution.

3.8 Circular Dichroism Spectroscopy

The CD spectrum of CT-DNA was recorded in the presence of increasing concentration of the complex $[Re(CO)_3(BBIB)Py]^+$. Without the complex present the spectrum is typical of B-DNA with a positive signal at 280 nm. As the complex is introduced, the DNA signal is observed to notable drop, with the appearance of two

new absorptions at 340 and 420 nm, in a region that can only be attributed to the complex itself. However the complex is achiral and should not be exhibiting a Cotton effect. This would indicate that on interaction with DNA it is then in a chiral environment where some binding to the DNA is shown. There is an indication that the a higher concentration of complex shows a stronger signal (Figure 33).

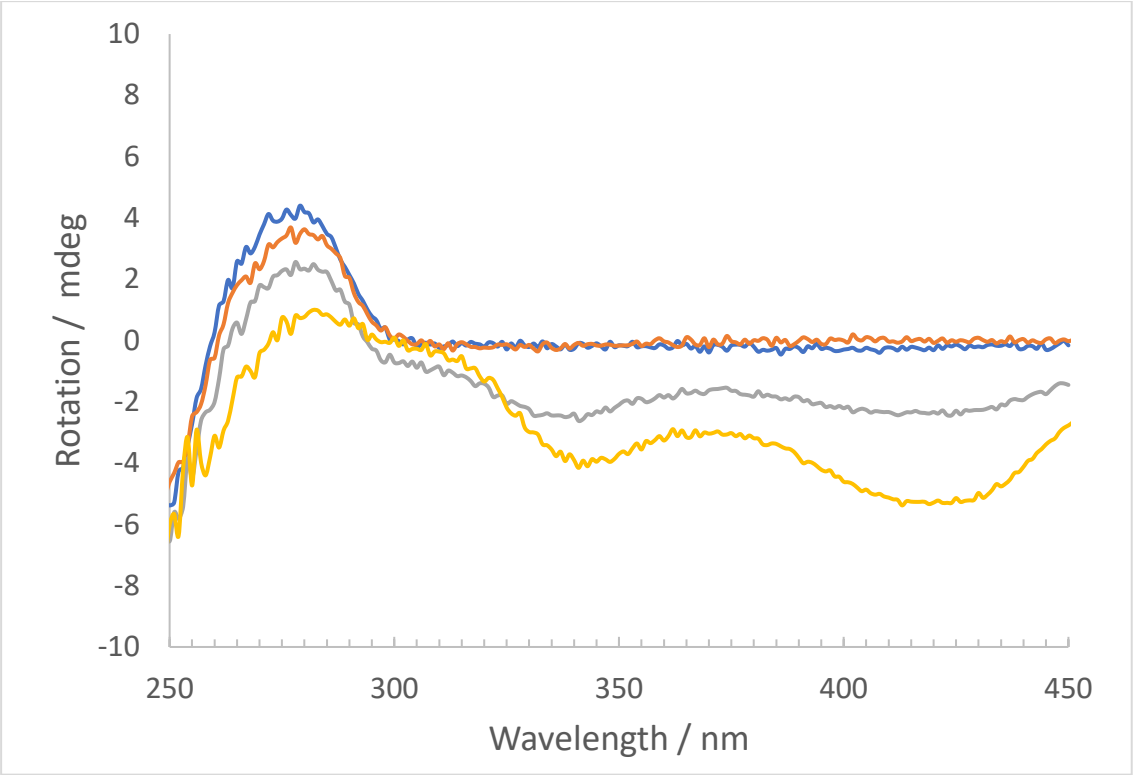

Figure 33: Circular Dichroism spectra of DNA and complex with increasing amounts of complex.

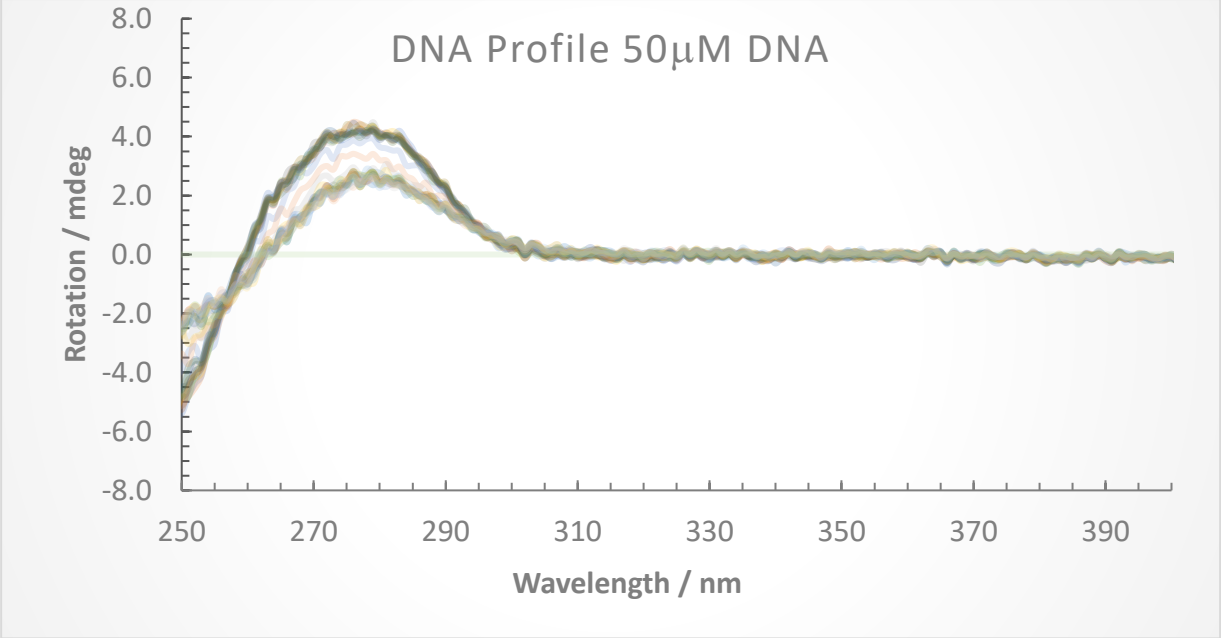

Figure 31: The Denaturation Circular dichroism spectra of DNA 50 μMol in DMSO / tris buffer solution.

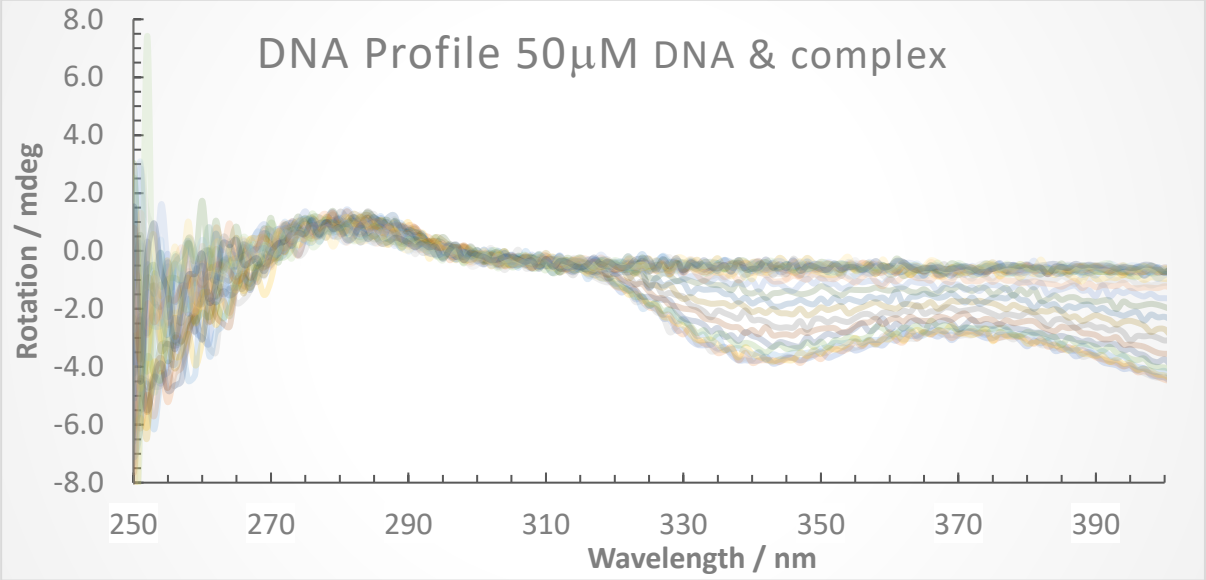

Figure 32: The denaturation circular dichroism spectra of DNA 50 μMol (bases) and $[Re(CO)_3Py(BBIB)]^+$ 50 μMol in DMSO / tris buffer solution.

However with the addition of DNA to $[Re(CO)_3T(BBOB)]^+$ and $[Re(CO)_3T(BBTB)]^+$ there is no cotton effect that is taking place. The complex is a chiral therefore this is expected therefore there is no interaction shown when introduced to DNA. Figure 33 indicates that after 300 nm there are no signals and the one at around 280 is typical of B-DNA.

A)

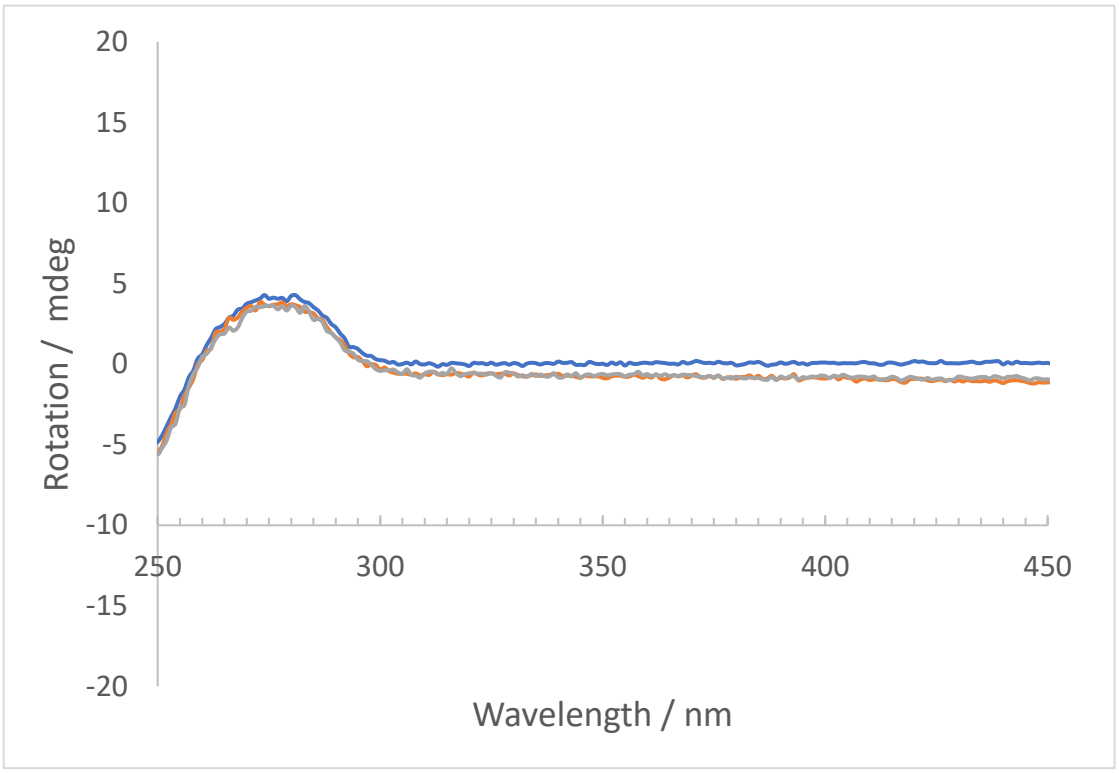

B)

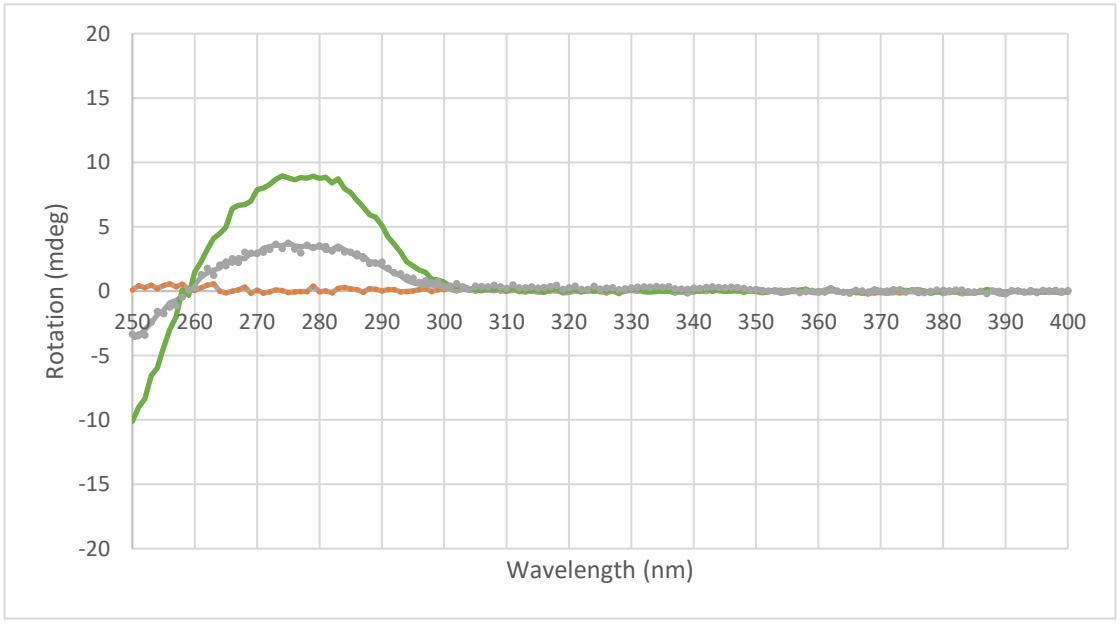

Figure 33: Denaturation circular dichroism spectra of DNA 50 μMol (bases and complex with increasing amounts of A) $[Re(CO)_3T(BBOB)]^+$ B) $[Re(CO)_3T(BBTB)]^+$ with 50 μMol in DMSO / tris buffer solution.

3.9 Thermal Denaturation Studies

The double helix is the dominant form of DNA, which is held together by strong bonds and when the DNA is heated the strands can be “unzipped” and the biopolymer denatures. The thermal denaturation studies portray the intensity of absorbance with increasing temperature. This change occurs at approximately 280 nm for DNA due to the π-π* interactions (figure 31). A change induced by binding would be indicated by a change in the absorbance, as well at the temperature at which the double helix splits into two strands. When a groove binding interaction has occurred it would be anticipated that there would be lowering in the temperature as there is less stability of the DNA to denaturation, whereas intercalation shows a large increase in melting temperature as there is more stability when it is bound to the double helix due to the additional π-stacking interactions. Some rhenium bipyridine complexes have been established to affect the melting temperature of DNA.

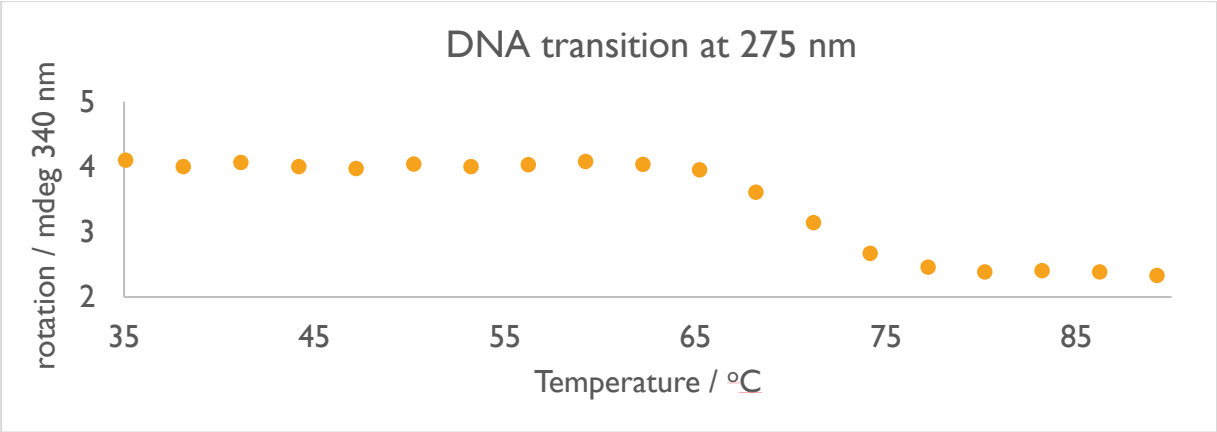

Figure 34: Melting curves of $[Re(CO)_3(BBIB)Py]^+$ with DNA at 275 nm

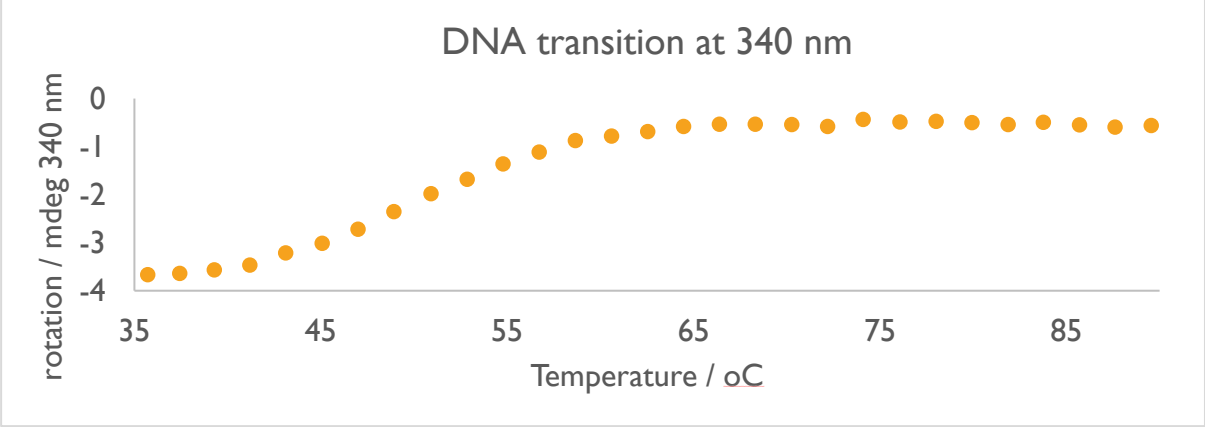

Figure 35: Melting curves of $[Re(CO)_3(BBIB)Py]^+$ with DNA at 340 nm

For the melting temperature of DNA itself (Figure 31), the transition occurs at 70 ^{o}C. However in the presence of the complex (Figure 32), there are two transitions evident at different wavelengths. At 275 nm, the transition is occurring at 70 C, and relates to the DNA denaturing (Figure 34). However, at 340 nm, there is a strong transition temperature occurring around 50 C (Figure 35) which portrays an interaction between the complex and DNA which is potentially the dissociation of the complex from the DNA. Hence the evidence would suggest that there is a very weak reversible binding between the complex and the DNA, with complex potentially dissociating from the DNA before the DNA denatures.

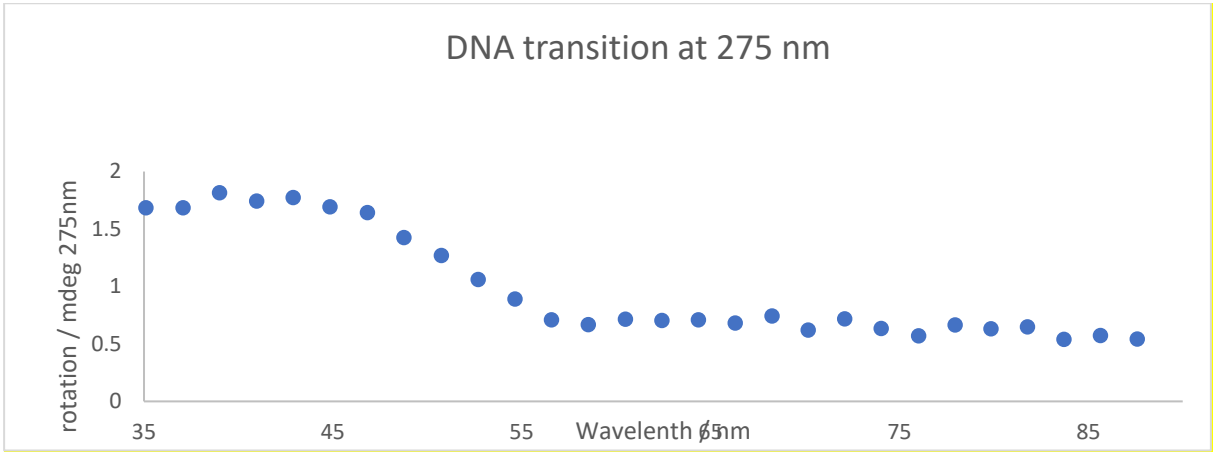

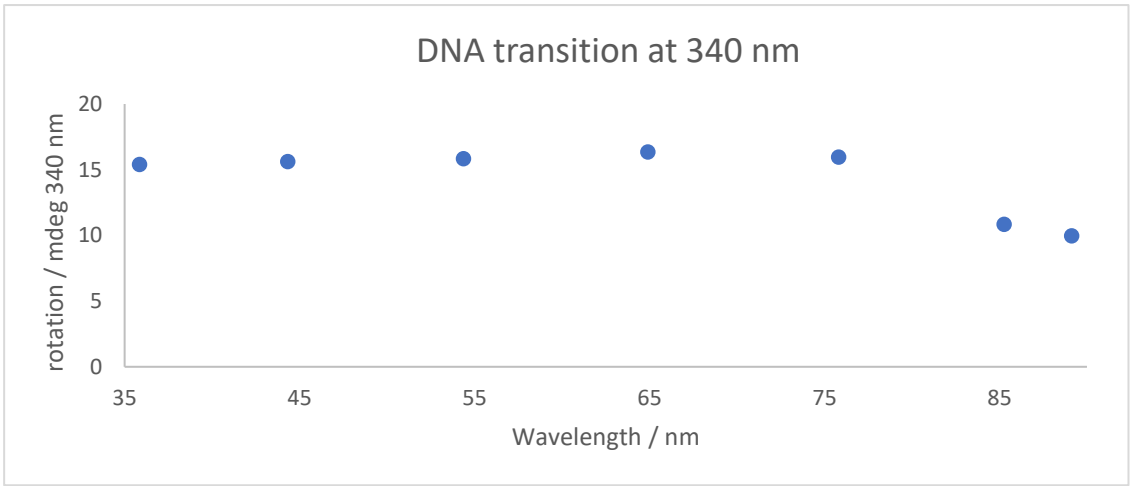

Figure 37: Melting curves of $([Re(CO)_3(BBTB)T]^+$ and with $([Re(CO)_3(BBTB)T]^+$ with 10µM DNA

However with $([Re(CO)_3(BBTB)Py]^+$ at 275 nm the transition occurs at 50 oc which means that there is initial dissociation of the complex from DNA and then the denaturation of DNA occurs at 70oC at 340 nm which means that the DNA has then denatures which indicates that there was no interaction between the DNA and complex as once added, it was dissociated right away.

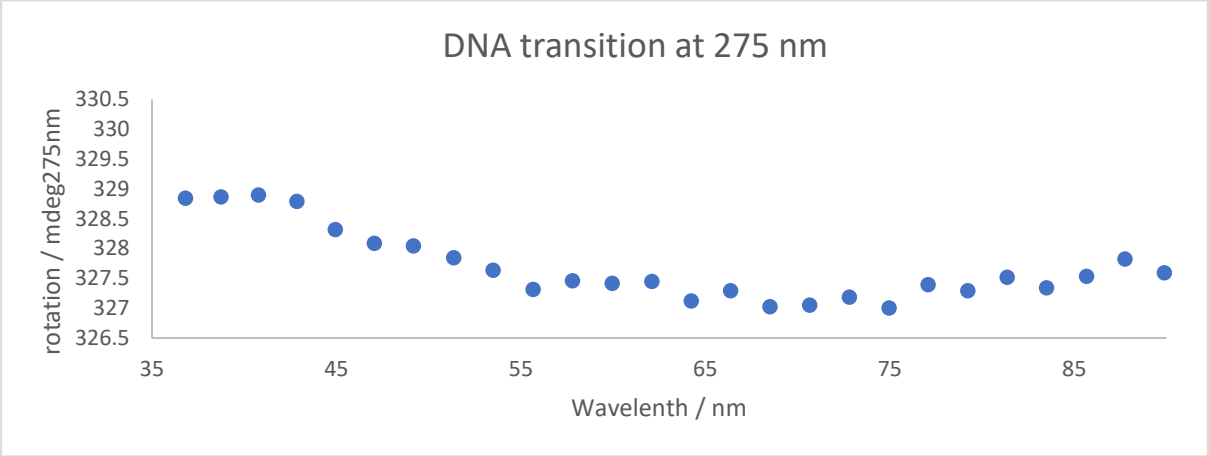

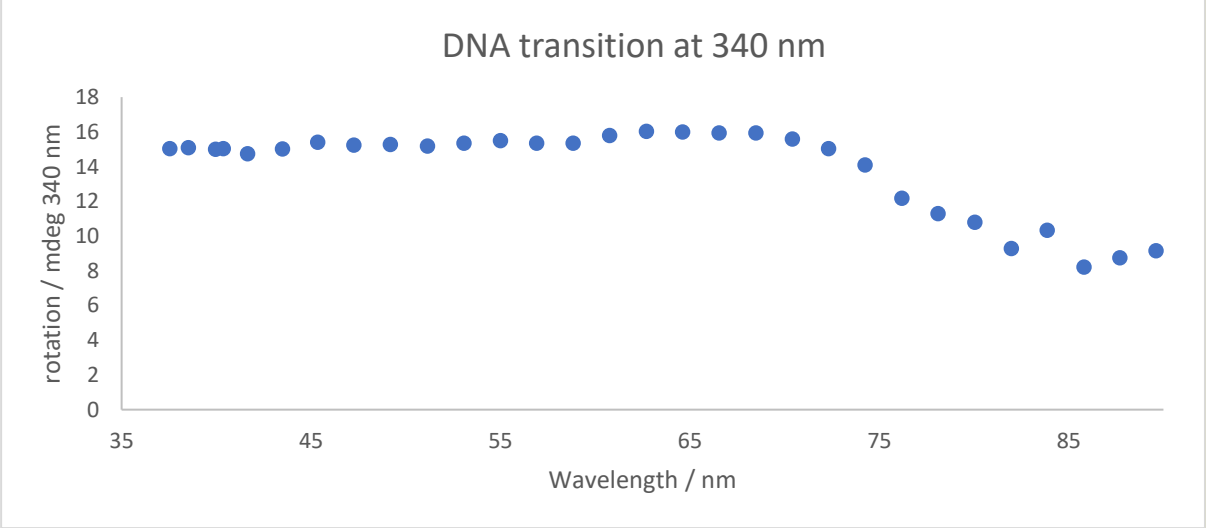

Figure 38: Melting curves of $([Re(CO)_3(BBOB)T]^+$ and with $([Re(CO)_3(BBOB)T]^+$ with 25µM DNA

A similar result also occurred with $([Re(CO)_3(BBOB)T]^+$ where the complex dissociated before the DNA denatured with the transition taking place at 50Oc at 275 nm and then at 340 nm at 70oc, indicating that no interaction took place with DNA.

Figure 39: Melting curves of ($[Re(CO)_3(BBIB)T]^+$ and with ($[Re(CO)_3(BBTB)T]^+$ with 50μM DNA

This shows that it could be possible that the complex loses interaction with DNA when making it more soluble.

3.12 Iridium complexes of BBOB, BBTB and BBIB

Due to the solubility issues and ligand displacement some work was carried out with iridium where the iridium complexes were synthesised and some DNA work was completed.

The synthesis of the iridium phenylpyridine complexes of BBOB, BBTB and BBIB were completed by heating the appropriate ligands with $\{Ir(ppy)_2(\mu\text{–}Cl)\}_2$ in DMSO at 120 ^oC overnight. This formed a dark orange/red solution. Once the resulting reaction was cooled, water was added which produced a precipitate and the complex was isolated by filtration. Similar to the rhenium compounds, the precipitate was very fine, and the isolation proved to be very slow, typically taking 16 hours to get the product to dryness. Alternatively, the materials could be isolated on Celite which and the crude product abstracted into methanol, although the celite tended to retain colour in the process. The crude product was then purified by column chromatography eluted with 70% acetonitrile and 30% toluene saturated with potassium nitrate. The column produced a major and minor product which were determined by NMR. The major band was stripped off the column by the addition of 20% methanol and the product was then obtained through recrystallisation, which was a dark orange precipitate as *N*,*N*'-*trans*-$[Ir(ppy)_2(BBOB)]NO_3$: 18%, $[Ir(ppy)_2(BBIB)]NO_3$: 31%, $[Ir(ppy)_2(BBTB)]NO_3$: 20% the minor product travelling in advance of the main. Fraction was believed to be the *cis*-isomer, having a far more complicated NMR spectrum.

In comparison to the rhenium complexes these complexes had good solubility in a range of solvents including acetone and methanol. Mass spectroscopy data indicated that the formation of all three of the iridium complexes had been completed through a M^+ peak at 887 for $[Ir(ppy)_2(BBIB)]NO_3$, 923.12 for $[Ir(ppy)_2(BBTB)]NO_3$ and 891 for $[Ir(ppy)_2(BBOB)]NO_3$.

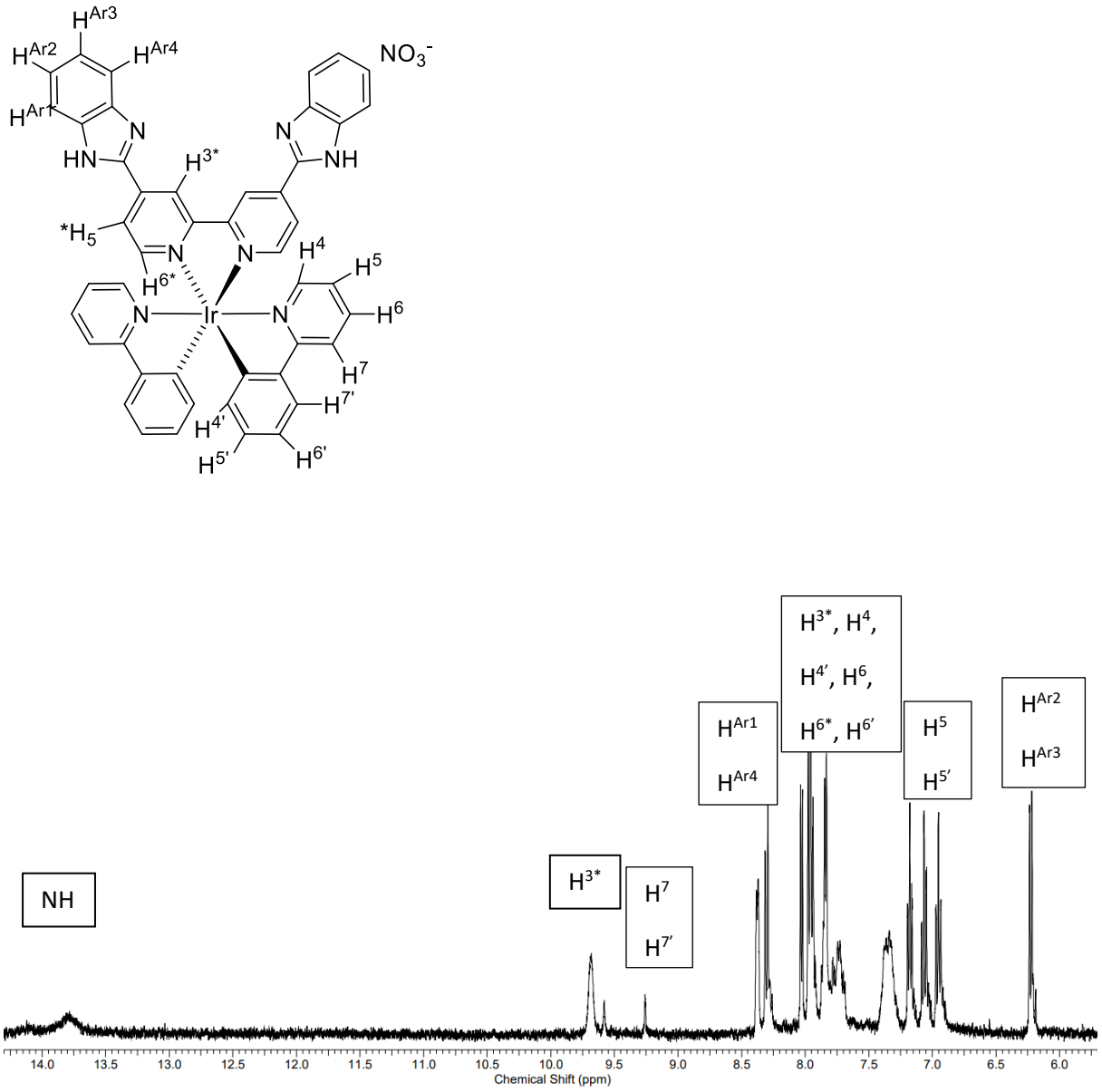

Figure 40: 1H NMR assignment of $[Ir(ppy)_2(BBIB)]NO_3$ in acetonitrile

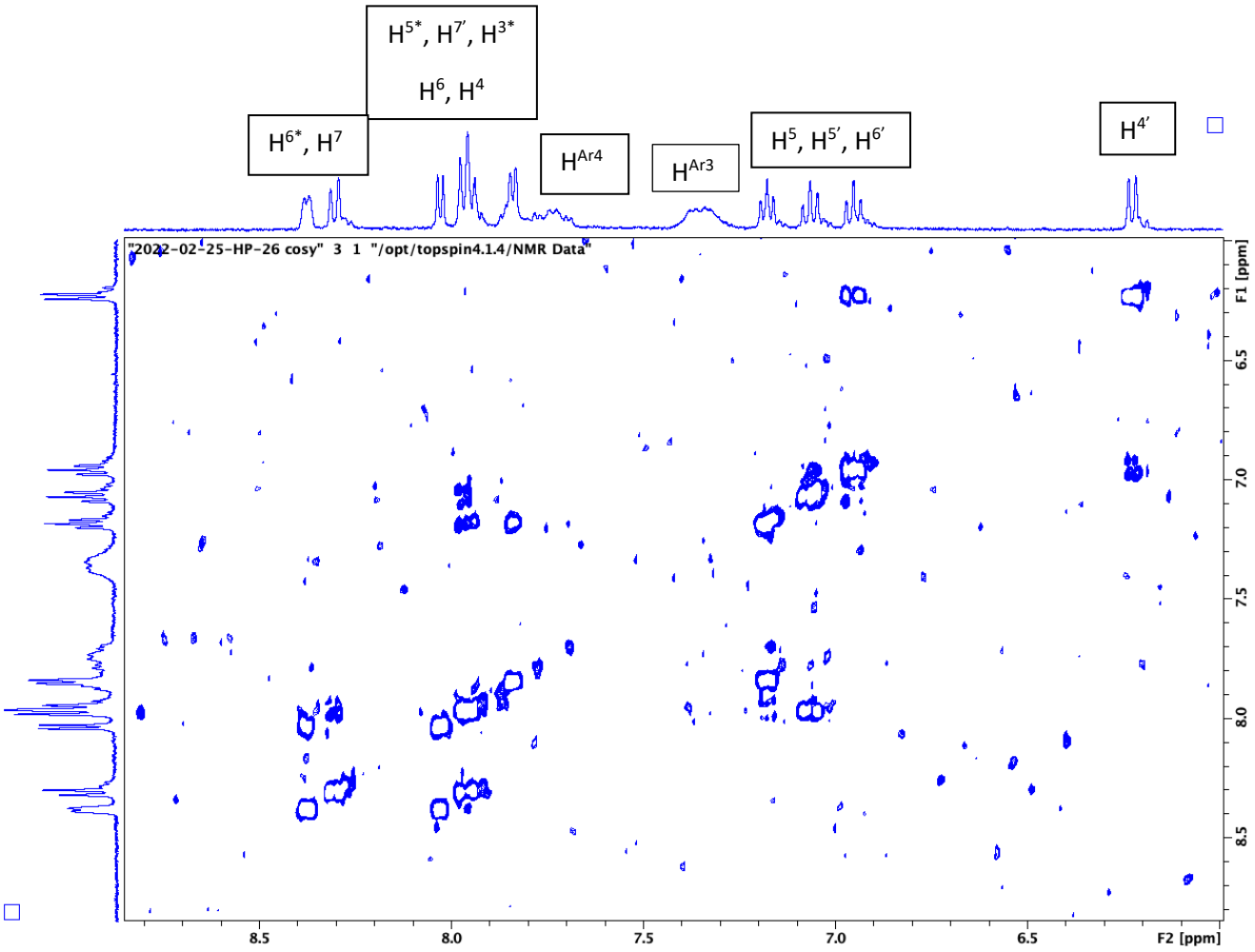

Figure 41: COSY assignment of $[Ir(ppy)_2(BBIB)]NO_3$ in acetonitrile.

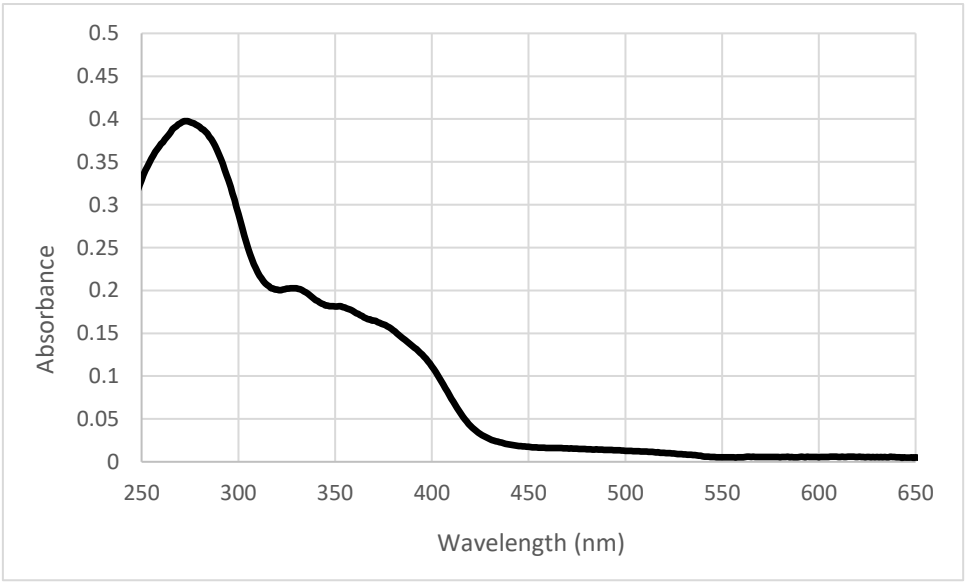

Figure 42: UV-Vis absorbance spectrum of $[Ir(ppy)_2(BBIB)]NO_3$ in acetonitrile

B)

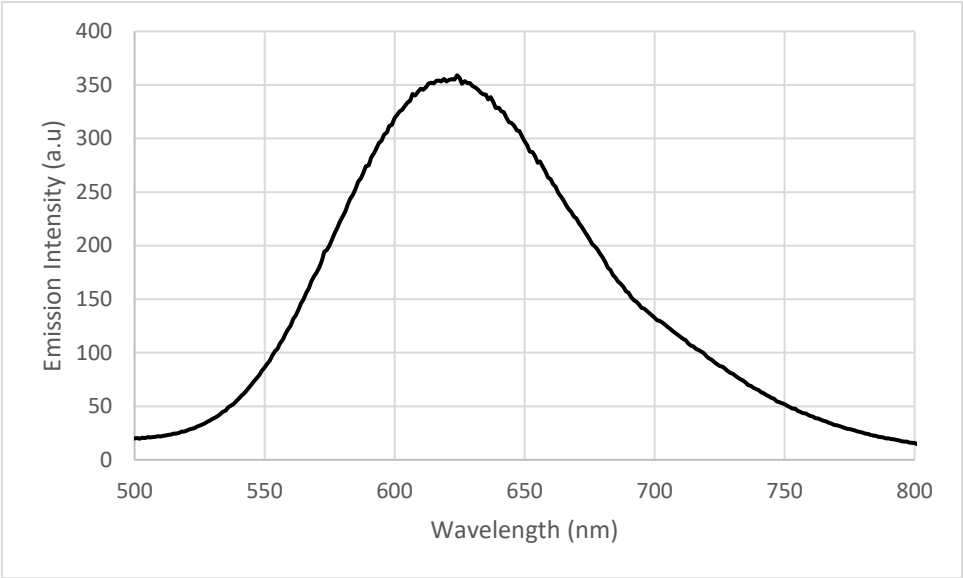

Figure 43: Emission spectrum of $[Ir(ppy)_2(BBIB)]NO_3$ in acetonitrile

	Absorption λ_{max} ± 1 nm	Emission λ_{max} ± 1 nm
$[Ir(ppy)_2(BBIB)]NO_3$	255	350
	325	
	400 (sh)	
$[Ir(ppy)_2(BBTB)]NO_3$	246	328
	320	
	460 (sh)	
$[Ir(ppy)_2(BBOB)]NO_3$	220	295
	330	
	390	

All three iridium complexes also showed a similar absorbance and emission spectra. The three absorbance peaks are present in the spectra as well as a reasonable phosphorescent which was shown by the complexes.

Further work to investigate whether these complexes could be used to bind DNA specifically were then considered. However, despite having far greater solubility than the analogous Re complexes, they had remarkably poor solubility in aqueous solution, even as the nitrate salts. The addition of tris buffer solution to the complexes dissolved in a small quantity of methanol, DMSO or DMF resulted in an immediate precipitation, and a colourless solution. As a consequence, further investigations with the complexes with CT-DNA could not be completed given the time constraints of the project and the availability of materials.

4. Conclusions

It has been shown that small changes to a molecule can have the potential to make substantial differences in the ability to interact with biological species. The DNA binding abilities are determined by: chirality, molecular shape, planarity, conjugation of ligands and hydrogen donors or acceptors, and ability of cations to interact with anions. This report has investigated the benzimidazole, benzoxazole and benzothiazole complexes when bound to rhenium and iridium. An interaction with DNA was found within the rhenium complexes as in contrast to the iridium complexes due to the solubility issues that were found.

UV-Vis and emission studies were completed which showed consistency throughout the project. The iridium complexes showed a higher fluorescence (evidence?). With the DNA studies, increasing the amount of DNA was not showing much difference and there was just a slight increase in emissive behaviour of the complexes.

Through the circular dichroism studies it was shown that when increasing the solubility of the complex through T, there was no interaction with DNA, however a slight interaction was shown with the pyridine version of the complex, with an unusual Cotton response of the bound complex $[Re(CO)_3(BBIB)Py]^+$.

5 Experimental

5.1 Materials

Acetone, acetonitrile, 1,2-phenylenediamine, 2-rhenium pentacarbonyl bromide and chloride, polyphosphoric acid, potassium carbonate, 1,2-thiophenol and tris(hydroxymethyl)-aminomethane (Tris) were obtained from Fisher Scientific. Silica (Merck) was used for purification of the iridium complexes. Tetrabutylammonium chloride was purchased from Sigma Aldrich). Acetone-D_6, D_2O, acetonitrile-D_3 and DMSO-D_6 were obtained from Fluorochem for use as solvents in NMR spectroscopy. Lyophilised calf thymus DNA (*ct*-DNA) was purchased from Merck for use in DNA binding studies.[46] $[Ir(ppy)(\mu\text{–}Cl)_2]_2$ was prepared by Nick Fletcher using a standard literature procedure.

5.2 Physical Measurements

NMR spectra were recorded on a Bruker Fourier 300 or a Bruker Avance III 400 at 298 K and referenced to TMS. The absorbance spectra were recorded on an Agilent Cary-60 UV-Vis spectrometer using a 1 cm path length quartz cuvette. The emission spectra were recorded on a Agilent Carey Eclipse UV-Vis spectrophotometer using a clear quartz cuvette. The circular dichroism (CD) spectra were recorded in acetonitrile or Tris buffer in a 1 cm cell on an Applied Photophysics Chirascan-plus CD Spectrometer. *ct*-DNA concentrations were determined from UV absorbance at 260 nm with an assumed average extinction coefficient of 6600 $M^{-1}cm^{-1}$.

5.3 Ligand Synthesis

5.3.1 Synthesis of 4,4'-Bis(benzoxazol-2-yl)-2,2'-bipyridine (BBOB)•H_3PO_4

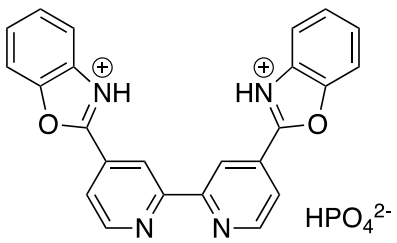

2-Aminophenol (1000 mg, 9.16 mmol), 4,4-dicarboxylic acid-2,2-bipyridine (1109 mg, 4.582 mmol) and polyphosphoric acid (approx.10 ml) were heated between 120°C to 150°C for 16 h. The resulting black viscous oil was added to water (100 ml), which resulted in a black precipitate, which was collected by filtration, and air dried. Yield = 0.881, 49%

^{1}H NMR (400 MHz, DMSO-D_6) d: 13.48 (2H, br, NH), 9.26 (2H, s, H^{bpy3}), 8.96 (2H, d, *J* = 5.2 Hz, H^{bpy6})

Mass spectroscopy: $[MH]^+$: 390.10 (theoretical value for $C_{24}H_{15}N_4O_2$: 391.40)
Infrared Spectroscopy: 3050 cm^{-1} (N-H stretch) 1342 cm^{-1} (C-N ring mode) 1310 (C-O stretching aromatic)

5.3.2 4,4'-Bis(benzimidazol-2-yl)-2,2'-bipyridine (BBIB)

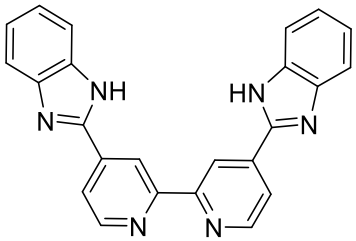

Using the same procedure as for BBOB, 1,2-phenylenediamine (560 mg, 5.178 mmol) and 4,4-dicarboxylic acid-2,2-bipyridine (627 mg, 2.589 mmol) and neutralised with saturated aqueous potassium carbonate was filtered which was collected by filtration, and dried. Yield = 0.593, 59%
^{1}H NMR (400MHz, DMSO-D_6): δ 9.26 (^{1}H, s), 8.96 (^{1}H, d, *J* = 5.1Hz), 8.25 (^{2}H, dd, *J* = 1.7, 5.1Hz) 7.70 (^{2}H, dd, *J* = 3.2, 5.8Hz) 7.30 (^{2}H, dd, *J* = 3.1, 6.0Hz)
Mass spectroscopy: $[MH]^+$: 390.46 (theoretical value for $C_{24}H_{17}N_4$: 388.42)
Infrared Spectroscopy: 3050 cm^{-1} (N-H stretch)

5.3.3 4,4'-Bis(benzothiazol-2-yl)-2,2'-bipyridine (BBTB)

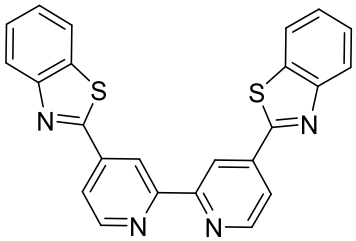

1,2-Thiophenol, (0.514 ml, 4.106 mmol), 4,4-dicarboxylic acid-4,4-bipyridine (723 mg, 2.053 mmol) were heated at 150 ^{o}C for 16 hrs. The product was extracted from the flask by washing with a saturated aqueous potassium carbonate solution and acetone resulting a brown precipitate which was allowed to stand for 48 hrs, and then collected by filtration. Yield: 0.562, 65%

1H NMR (400 MHz, DMSO-D6): δ 9.26 (1H, s, H3*), 9.10 (1H, d, *J* = 5.6 Hz, H^{6*}), 8.39 (1H, dd, *J* = 1.5, 5.6 Hz, H^{5*}), 8.31 (1H, d, *J* = 6.7 Hz, $H^{ar1\ or\ ar4}$), 8.10 (1H, d, *J* = 8.7 Hz, $H^{ar1\ or\ ar4}$), 7.73 (1H, dt, *J* = 1.3, 7.2, 15.3 Hz, $H^{ar2/3}$), 7.64 (1H, dt, *J* = 1.4, 8.1 15.2 Hz, $H^{Ar2/3}$)

Mass spectroscopy: $[MH]^+$: 423.61 (theoretical value for $C_{24}H_{14}N_4S_2$: 422.52)

5.4 $[Re(CO)_3(L)Br]$ (where L is BBOB, BBIB and BBTB)

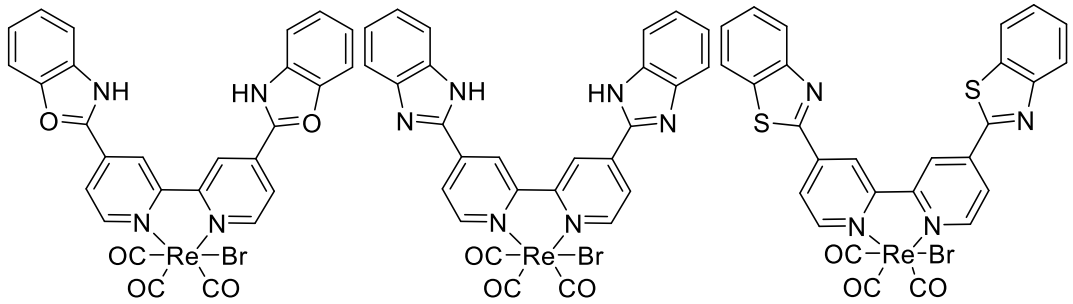

The ligand, BBTB (156mg 0.369mmol), BBOB (140 mg, 0.359 mmol), BBIB (146 mg, 0.377 mmol) and $Re(CO)_5Br$ (0.150 mg, 0.369 mmol), (0.146 mg, 0.259 mmol), (153 mg, 0.377 mmol) were heated at 120°C in DMSO (10 ml) . The orange solution was poured in water (70 ml typically) resulting in an orange precipitate which was collected by Hirsch filtration.

$[Re(CO)_3(BBOB)Br]$

Yield = 1.371 g, 50%

$[Re(CO)_3(BBTB)Br]$

Yield = 0.151 g, 53%

$[Re(CO)_3(BBIB)Br]$

Yield = 0.211 g, 76%

5.5 $[Re(CO)_3(L)py]Cl$ (where L is BBOB, BBIB and BBTB)

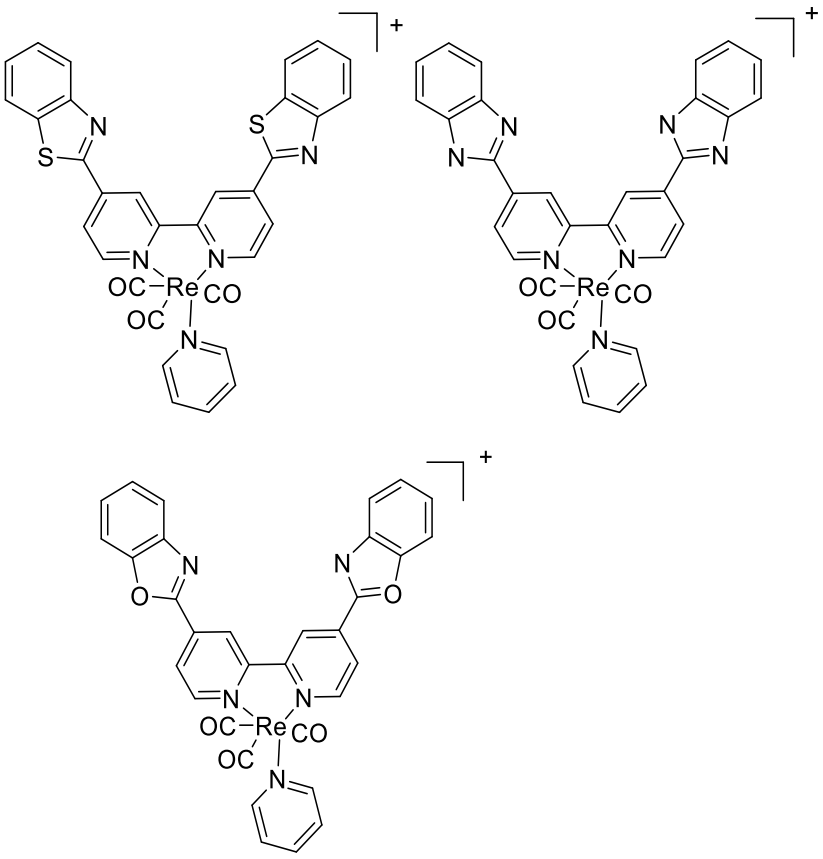

In order to make it soluble to carry out DNA work we added a pyridine group. The procedure was as follows: $[Re(CO)_3(L)Br]$ where L = BBTB, BBOB and BBIB) was heated with pyridine and silver nitrate for 3 hours. Either tetrabutylammonium chloride, sodium chloride or silver perchlorate (0.1g) were then added which was left to stir for 15-20 mins. This was filtered through Celite® under nitrogen, and washed using methanol, before the solvent was evaporated to dryness giving a yellow solid.[25]

$[Re(CO)_3(BBOB)Py]Cl$

Yield = 0.0484 g, 37%

$[Re(CO)_3(BBIB)Py]BF_4$

Yield = 0.0303 g, 27%

$[Re(CO)_3(BBTB)Py]Cl$

Yield = 0.0723 g, 59%

5.6 Alternate method:

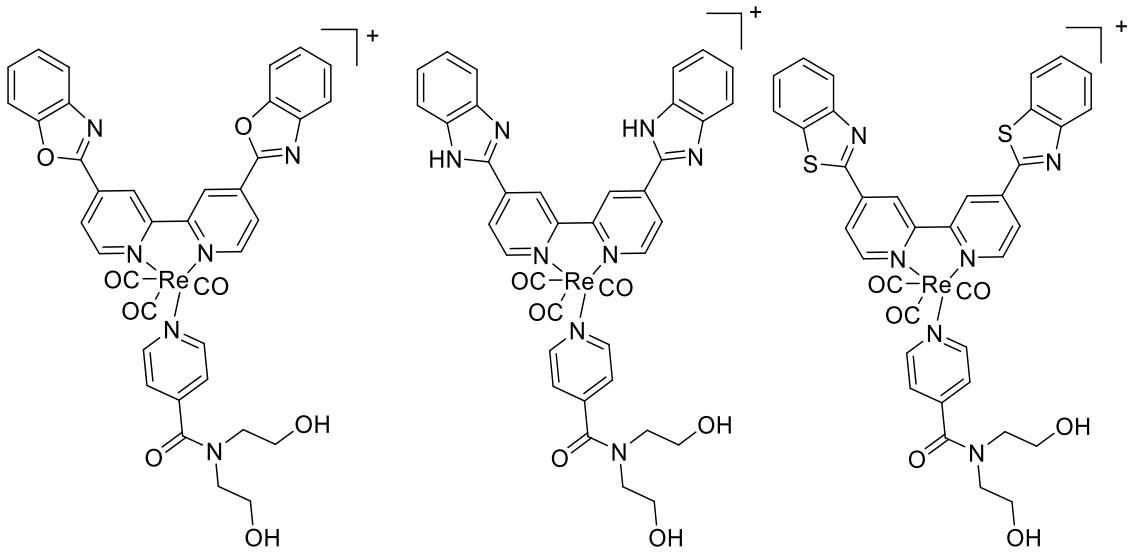

$[Re(CO)_3(L)Br]$ where L = BBTB, BBOB and BBIB) were dissolved in acetonitrile (20 ml) and $AgBF_4$ were left on reflux for 16 hours under nitrogen to form $[Re(CO)_3L(NCMe)]BF_4$. The reaction mixture was filtered through Celite® and the acetonitrile was evaporated under vacuum. The yellow solid was dissolved in THF and the ligand was added and refluxed for 3 h. The solvent was removed, and dissolved in the minimum amount of methanol and the product precipitated by the addition of a saturated solution of KPF_6. The product was isolated on Celite® and removed by dissolving in methanol. This was completed for $Re(CO_3)$(BBOB,BBIB&BBTB)Br.

$[Re(CO)_3(BBOB)T]PF_6$

Yield = 35%

$[Re(CO)_3(BBIB)T]$

Yield = 0.0113g, 40%

$[Re(CO)_3(BBTB)T]$

Yield = 0.0121 g, 44%

5.7 Iridium Complexes

$[Ir(ppy)_2L]NO_3$

The thiazole ligand (100 mg, 0.237 mmol) and $[Ir(ppy)(\mu\text{-}Cl)_2]_2$ (525mg, 0.490 mmol) in DMSO (5 ml) were heated for 16 hours. This was diluted with water giving an orange precipitate, which was collected by filtration and left for 16 h to dry. The crude product was purified by column chromatography eluted with 30% toluene and 70% acetonitrile, saturated with potassium nitrate. The major band was stripped off the column by the addition of 20% methanol, the product was obtained via recrystallization from aqueous acetone as the nitrate salt. Yield = 0.051g, 20%
The same procedure was carried out by the oxazole and the thiazole.

$[Ir(ppy)_2(BBOB)]NO_3$
Yield = 0.039g, 18%

$[Ir(ppy)_2(BBIB)]NO_3$
Yield = 0.0691, 31%

$[Ir(ppy)_2(BBTB)]NO_3$
Yield = 0.0691, 31%

5.8 Binding of Rhenium complexes to Calf Thymus DNA

Lyophilised calf thymus DNA (ct-DNA) was purchased from Sigma. This was diluted in Tris-Buffer. The concentration of ct-DNA per base pair was determined using the extinction coefficient of 6600 molar $base^{-1}cm^{-1}dm^3$ at 260 nm. Stock solution were prepared of all reagents.

The absorbance spectra were analysed between 200 and 600 nm. The fluorescence was between 500 and 900 nm and circular dichroism studies of the racemic complexes were recorded between 200-600 nm. DNA has an absorbance of 300 nm and the fluorescence intensity of complexes was measured in a 1 cm quartz cell between 550-800 nm with a excitation wavelength of 450 nm. Circular dichroism of the racemic complexes were recorded between 200-600 nm and all experiments were completed at room temperature. Emission quantum yields were completed in aqueous solutions at room temperature and relative to a aqueous solution of $[Ru(bpy)_3]^{2+}$.

5.9 Thermal Denaturation Experiments

Melting temperatures of ct-DNA (50 µm) were recorded with and without the presence of racemic complexes (35-85 nm) through the use of a CD spectrometer. The data was processed through the use of Microsoft Excel.

6 References

1. J. D. Watson and F. H. C. Crick, 1953
2. Zephyris, DNA, https://en.wikipedia.org/wiki/DNA).
3. M. H. Shamsi and H.-B. Kraatz, *J. of Inorg. and Organomet. Polymers and Mater.*, 2012, **23**, 4-23.
4. D. L. Morris, *BioMol. concepts*, 2014, **5**, 397-407
5. D. L. Ang, Benjamin J. Pages, E. P.Wright and J. R. Aldrich-Wright, *Dalton Trans*, 2015, 44, 3505
6. N. Ma and A. van der Vaart, *J. Am. Chem. Soc.*, 2016, **138**, 9951-9958.
7. A-B-Z-DNA, https://en.wikipedia.org/wiki/File:A-B-Z-DNA_Side_View.png).
8. I. Khalaila, A. Bergamo, F. Bussy, G. Sava and P. J. Dyson, *Int. J. Oncol.*, 2006, **29**, 261-268.
9. L. J. Boerner and J. M. Zaleski, *Curr. Opin. Chem. Biol.*, 2005, **9**, 135-144.
10. A. T. Krueger and E. T. Kool, *Curr. Opin. Chem. Bio.l*, 2007, **11**, 588-594.
11. C. L. Kielkopf, S. White, J. W. Szewczyk, J. M. Turner, E. E. Baird, P. B. Dervan and D. C. Rees, *Science*, 1998, **282**, 111-115.
12. A. Lauria, A. Montalbano, P. Barraja, G. Dattolo and A. M. Almerico, *Curr. Med. Chem.*, 2007, **14**, 2136-2160.
13. L. Strekowski and B. Wilson, *Mutat. Res.*, 2007, **623**, 3-13.
14. E. A. Plummer. K. K. Patel, M. Darwish, A. Rodger, M. J. Hannon, 2002, **91**, 229-229
15. S. M. Nelson, L. R. Ferguson and W. A. Denny, *Mutat Res*, 2007, **623**, 24-40.
16. Y. Yang, G. Liao and C. Fu, *Polymers*, 2018, **10**, 650
17. M. B. Ismail, I. N. Booysen and M. P. Akerman, *Nucleosides Nucleotides Nucleic Acids*, 2019, **38**, 950-971.
18. V. R. Cooper. Shen Li, T. Thonhauser, Bengt I. Lundqvist, and David C. Langreth, *J. Phys. Chem*., 2009, **113**, 11166-11172
19. H. D. Stoeffler, N. B. Thornton, S. L. Temkin and K. S. Schanze, *J. Am. Chem. Soc.*, 1995, **117**, 7119-7128.
20. L. Andrezalova and Z. Orszaghova, *J Inorg Biochem*, 2021, **225**, 111624.
21. M. Howe-Grant and S. J. Lippard, *Biochemistry*, 1979, **18**, 5762-5769.
22. D. S. Sigman, T. W. Bruice, A. Mazumder and C. L. Sutton, *Acc. Chem. Res.*, 1993, **26**, 98-104.
23. O. Nováková, J. Kaspárková, O. Vrána, P. M. van Vliet, J. Reedijk and V. Brabec, *Biochem*, 1995, **34**, 12369-12378.
24. C. Tan, S. Lai, S. Wu, S. Hu, L. Zhou, Y. Chen, M. Wang, Y. Zhu, W. Lian, W. Peng, L. Ji and A. Xu, *J. Med. Chem.*, 2010, **53**, 7613-7624.

25. K. K.-W. Lo, M.-W. Louie and K. Y. Zhang, *Coord. Chem.*, 2010, **254**, 2603-2622.
26. A. T. Hoye, J. E. Davoren, P. Wipf, M. P. Fink and V. E. Kagan, *Acc. Chem. Res.*, 2008, **41**, 87-97.
27. G. K. Tofaris, *Mov Disord*, 2012, **27**, 1364-1369.
28. M. M. Mohamed and B. F. Sloane, *Nat Rev Cancer*, 2006, **6**, 764-775.
29. S. Zhang, M. Hosaka, T. Yoshihara, K. Negishi, Y. Iida, S. Tobita and T. Takeuchi, *Cancer Res*, 2010, **70**, 4490-4498.
30. K. Koike, N. Okoshi, H. Hori, K. Takeuchi, O. Ishitani, H. Tsubaki, I. P. Clark, M. W. George, F. P. A. Johnson and J. J. Turner, *J. Am. Chem. Soc.*, 2002, **124**, 11448-11455.
31. M. S. Lowry, W. R. Hudson, R. A. Pascal and S. Bernhard, *J. Am. Chem. Soc.*, 2004, **126**, 14129-14135.
32. K. K. Lo, C. K. Chung and N. Zhu, *Chemistry*, 2006, **12**, 1500-1512.
33. S. K. Tripathy, U. De, N. Dehury, S. Pal, H. S. Kim and S. Patra, *Dalton Trans.*, 2014, **43**, 14546-14549.
34. F. L. Thorp-Greenwood, M. P. Coogan, L. Mishra, N. Kumari, G. Rai and S. Saripella, *New J. Chem.*, 2012, **36**, 64-72.
35. D. L. Ma, C. M. Che, F. M. Siu, M. Yang and K. Y. Wong, *Inorg. Chem.*, 2007, **46**, 740-749.
36. A. B. Tamayo, S. Garon, T. Sajoto, P. I. Djurovich, I. M. Tsyba, R. Bau and M. E. Thompson, *Inorg. Chem.*, 2005, **44**, 8723-8732.
37. S. Sreedharan, A. Sinopoli, P. J. Jarman, D. Robinson, C. Clemmet, P. A. Scattergood, C. R. Rice, C. G. W. Smythe, J. A. Thomas and P. I. P. Elliott, *Dalton Trans.*, 2018, **47**, 4931-4940.
38. S. Lin, L. Lu, T. S. Kang, J. L. Mergny, C. H. Leung and D. L. Ma, *Anal Chem*, 2016, **88**, 10290-10295.
39. F. B. H. Kether, F. Jemmezi, I. Amri, J. Bassem, J. Khiari, J. App, Chem, 2014, **7**, 2278-5736
40. O. Ajani, D. Aderohunmu, S. Olorunshola, C. Ikpo and I. Olanrewaju, *Orient. J. Chem.*, 2016, **32**, 109-120.
41. B. P. Nagori. P. Lokwani, N. Batra, A. Goyal, S. Gupta and N. Singh, *J. Chem. Pharm. Res.* , 2011, 302-311.
42. P. R. Dirisinala and N. K. Podila, J. App. Chem, 2020, **13** 14-26.
43. C. Spillane, "Synthesis of Ruthenium(II) Complexes as Potential Photoactive Minor Groove Binders" PhD Thesis, Queen's University Belfsast, 2005.
44. C. L. Howells, "Investigating Benzimidazole-Based Fluorophores for Their Biological Activities", PhD Thesis, Lancaster University, 2022.

45. J. Muldoon, A. E. Ashcroft and A. J. Wilson, *Chemistry*, 2010, **16**, 100-103.
46. M. Wrighton and D. L. Morse, *J. Am. Chem. Soc.*, 1974, **98**, 998-1003.
47. A. L. Blackburn, N. A. C. Baker, N. C. Fletcher, RSC Adv., 2014, **4**, 18442-18452.